DPST-78-128-7/8

SAVANNAH RIVER LABORATORY MONTHLY REPORT

^{238}Pu FUEL FORM PROCESSES JULY/AUGUST 1978

SAVANNAH RIVER LABORATORY
AIKEN, SOUTH CAROLINA 29801

PREPARED FOR THE U.S. DEPARTMENT OF ENERGY UNDER CONTRACT AT(07-2)-1

DISCLAIMER

DISCLAIMER

DPST-78-128-7/8

SAVANNAH RIVER LABORATORY MONTHLY REPORT

^{238}Pu FUEL FORM PROCESSES

JULY/AUGUST 1978

Approved by:

R. T. Huntoon, Research Manager
Nuclear Materials Division

E. I. DU PONT DE NEMOURS AND COMPANY
SAVANNAH RIVER LABORATORY
AIKEN, SOUTH CAROLINA 29801

PREPARED FOR THE U. S. DEPARTMENT OF ENERGY UNDER CONTRACT AT(07-2)-1

CONTENTS

FOREWORD

This report is one of a series to summarize progress in the Savannah River ^{238}Pu Fuel Form Program. This program is supported primarily by the DOE Division of Advanced Systems and Materials Production (DASMP), and also by the Division of Military Applications (DMA).

Goals of the Savannah River Laboratory (SRL) program are: to provide technical support for the transfer of DASMP and DMA ^{238}Pu fuel form fabrication operations from Mound Laboratory to new facilities at the Savannah River Plant (SRP), to provide the technical basis for ^{238}Pu scrap recovery at SRP, and to assist in sustaining plant operations. This part of the program includes:

Demonstration of processes and techniques, developed by the Los Alamos Scientific Laboratory (LASL) and Monsanto Research Corporation (MRC), for production at SRP. Information from the demonstration will provide the technical data for technical standards and operating procedures.

Technical Support to assist plant startup and to ensure continuation of safe and efficient production of high-quality heat-source fuel.

Technical Assistance after startup to accommodate changes in product and product specifications, to assist user agencies in improving product performance, to assist SRP in making process improvements that increase efficiency and product reliability, and to adapt plant facilities for new products.

MULTI-HUNDRED WATT PROCESS DEVELOPMENT

PuFF PARAMETRIC STUDY

Microstructural analysis of pellets made in the PuFF parametric experiment is in progress. Results, summarized below, will be discussed in the next two bimonthly reports.

All of the heat-treated pellets cracked. Cracks are being analyzed in an attmept to relate incidence of cracking to process conditions, microstructure, and density. Examination of as-pressed pellets is planned following completion of heat-treated pellets.

A statistical analysis of metallographic densities of the core regions, excluding cracks, was made because of concern about the effect of cracks on the interpretation of the bulk density data.[1] Results of this analysis indicate that hot press load had the largest effect on core density; feed powder mode size and hot press temperature also had significant effects. Higher densities resulted from high loads, high hot press temperature, and large mode size. Force application rate and shard sintering temperature showed smaller effects. These results correlate reasonably well with results of the bulk density analysis.[1]

Force application rate, in combination with high pressing load, affected the homogeneity of the pellet microstructure. Application of a high load at a fast rate (~10 sec), both comparable to original LASL pressing conditions, produced inhomogeneous microstructure with large density gradients. Improved homogeneity occurred at the lower hot pressing load and rate conditions.

PROCESS DEVELOPMENT FOR SPACE APPLICATIONS

DIRECT FABRICATION – Pu(IV) OXALATE PRECIPITATION TESTS

Additional tests were performed to determine the cause of the small particle size and inferior morphology observed for $^{238}PuO_2$ feed produced in SRP precipitations of Pu(IV) oxalate. Eleven ^{239}Pu(IV) and ^{238}Pu(IV) oxalate precipitations were made on a small scale under various conditions, and the calcined PuO_2 powders were characterized. Variables tested were stirring rate, precipitation temperature, nitric acid concentration, Pu concentration, the presence of seed crystals, and radiolysis due to ^{238}Pu decay. Results of these tests indicate that none of the conditions tested cause the abnormally fine particles and large agglomerates that exist in plant-scale feed. In fact, these tests continue to suggest that Pu(IV) precipitation is much more tolerant of variations in process conditions than is the present Pu(III) precipitation.

About 1200 g of $^{238}PuO_2$ were produced by calcining Pu(IV) oxalate from reverse-strike precipitations in HB-Line. The oxide was made to test production capability and to provide feed to fabricate test fuel forms by direct fabrication (direct hot pressing of feed powder). PuO_2 powder made in the six production runs showed less than the desired characteristics.[3] Production powders typically contained large (up to 0.25 in.) agglomerates of small (1 to 2 μm) particles comprising about 50% of the powder, ∿25% of small and poorly formed prisms and aggregates, and about 25% of the desired 10 to 20-μm prismatic particles that were obtained in all laboratory-scale precipitations.

The fabrication response of this production feed is being evaluated with small pellets in the AMF before testing on MHW spheres in the PEF. Initial results reported in the March-April 1978 report[2] showed MHW pellets could still be made directly, but adjustments to the powder might be required to prevent shrinkage to densities high enough (>85% TD) to cause fracture on oxidation. The precipitation tests reported here were performed concurrently with the fabrication evaluation to determine why production-scale precipitation produced fines and agglomerates.

The eleven precipitation tests are summarized in Table 1. The variables tested were selected on the basis of their traditional role in promoting excessive nucleation rate (excess fines) or agglomeration and on the basis of known variations in the plant processing.[2] All precipitations were performed in laboratory facilities on a 1-gram scale. The calcined powders were characterized for particle size distribution (Figure 1) with a Coulter Counter* and for morphology by scanning electron microscopy (Figures 2-15) and light microscopy.

TABLE 1

Tests of Effects of Pu(IV) Oxalate Precipitation Variables on PuO_2 Characteristics[a]

Variable	*Sample*[b]	*Level of Variable*	*Mass Mode Size, μm*	*Size and Morphology*
Heel	Z-1	Control Standard	13	Unimodal, normal prisms
Heel	Z-2	Residual Slurry from Z-1	15	Unimodal, normal prisms
Isotope, B-Line Feed	P-1	^{238}Pu vs. ^{239}Pu[c]	8 to 13	Smaller prisms, small aggregates
Stirring Rate	T-2M	No stirring	19	Unimodal, normal prisms
Stirring Rate	T-2D	150 rpm	27	Unimodal, more larger prisms
Stirring Rate	T-2E	900 rpm	17	More smaller platy particles, rounded corners on prisms
Pu Concentration	T-2F	10g/l	18	Unimodal, well developed prisms, Most desirable characteristics
Nitric Acid Concentration	T-2G	2.2M	17	Unimodal, tendency for more fines
Nitric Acid Concentration	T-2H	0 5M	20	Unimodal; extensive rounding of prisms
Precipitation Temperature	T-2K	25 to 31 to 25°C	19	Rounded prisms, some aggregates
Precipitation Temperature	T-2L	35 to 28 to 35°C	19	Rounded prisms, some aggregates

a. Standard Laboratory Conditions — Pu concentration in feed, 5g/l; Nitric acid concentration in feed, 1 1M; Precipitation temperature, 25 ± 1°C; Stirring rate, 400 ± 50 rpm

b. All ^{239}Pu except Sample P-1

c. 6 g Pu/L vs 5 g Pu/L in laboratory preparations

* Product of Coulter Corp., Hialeah, Fla.

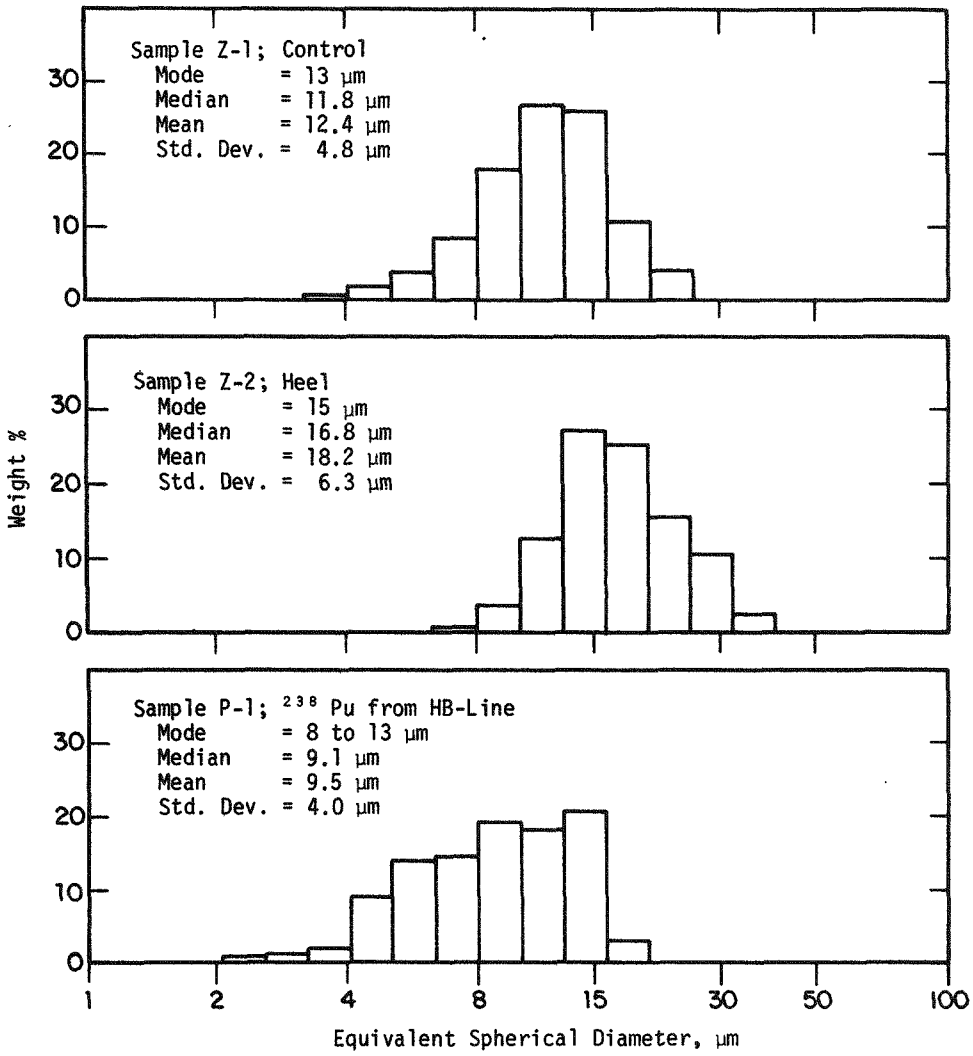

FIGURE 1. Mass Particle Size Distribution of PuO_2 Produced in Tests of Pu(IV) Oxalate Precipitation

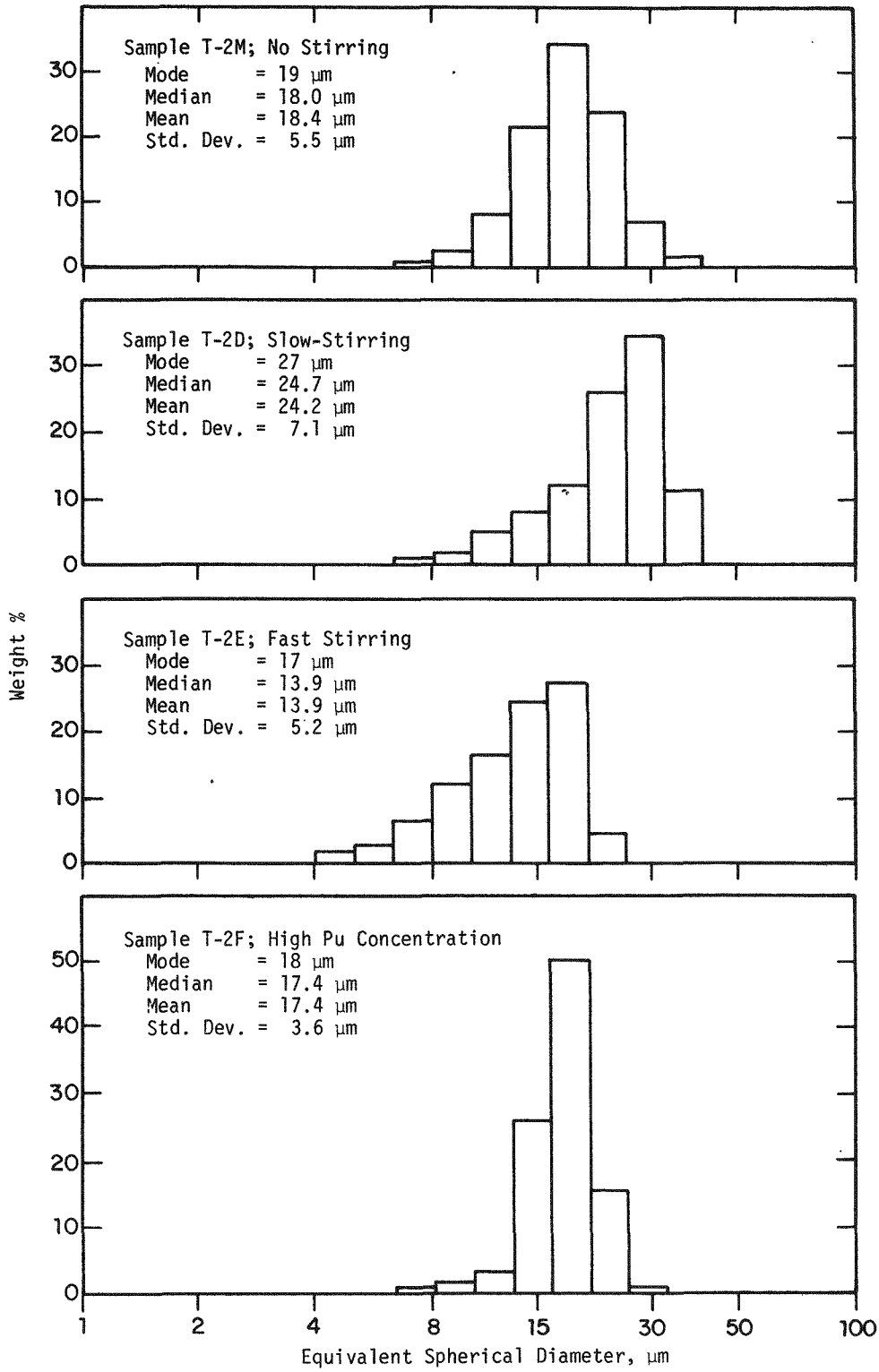

FIGURE 1. (Continued)

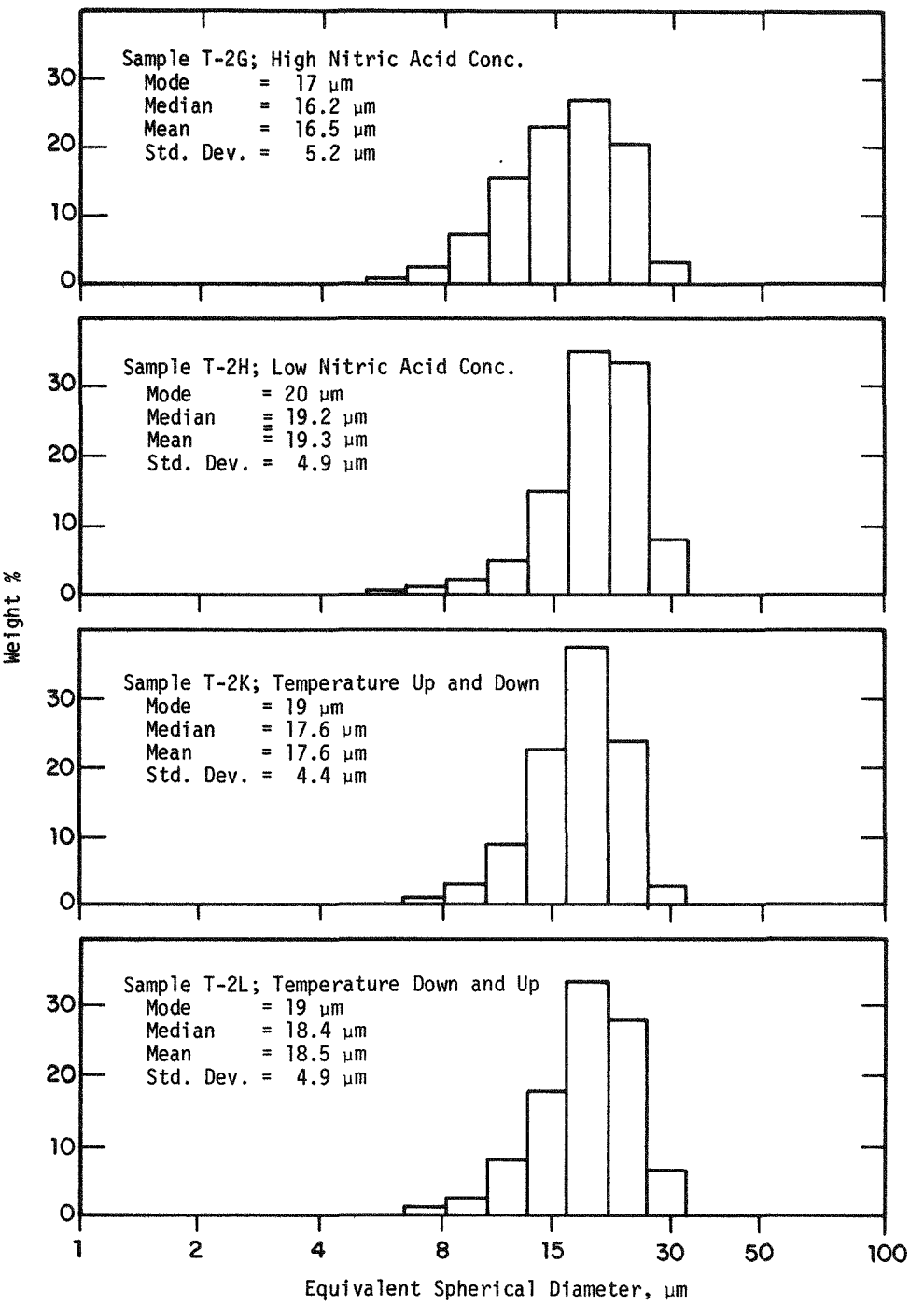

FIGURE 1. (Continued)

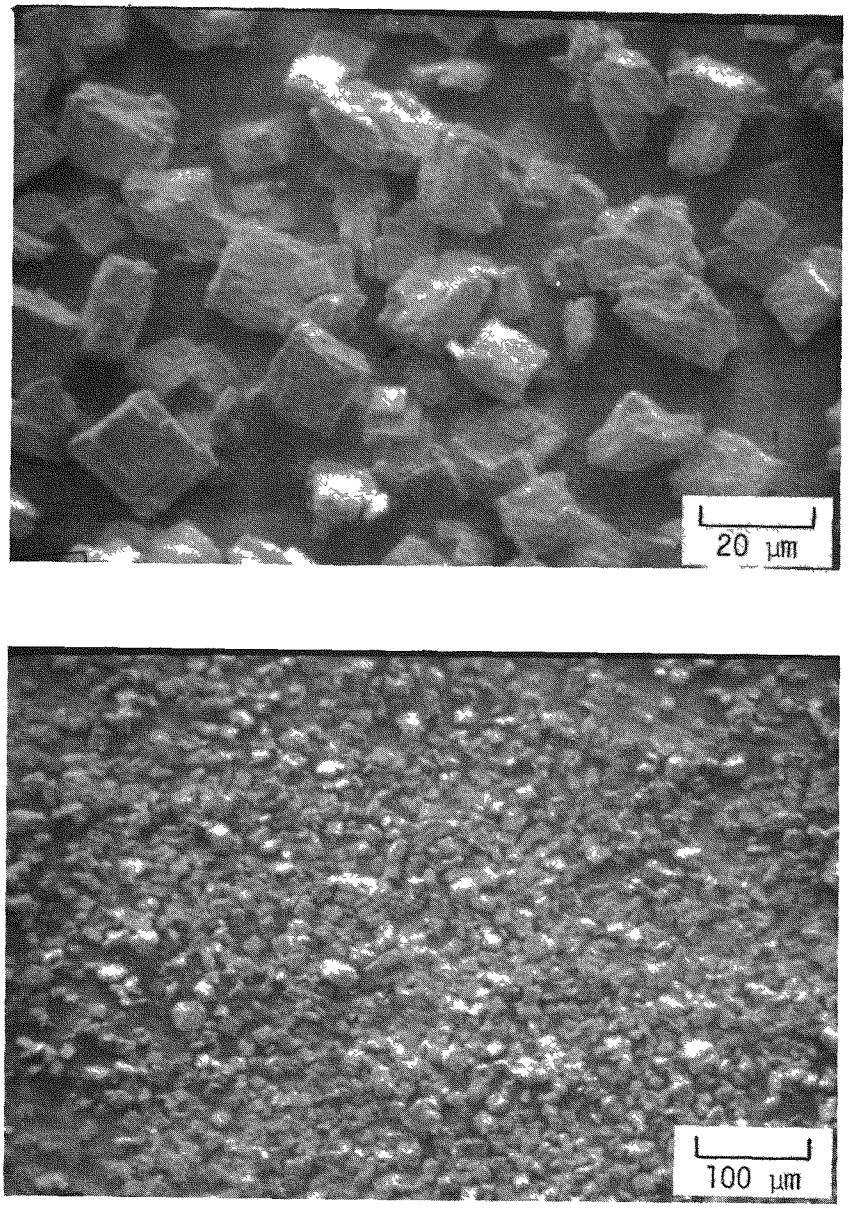

FIGURE 2. $^{239}PuO_2$ Produced by Pu(IV) Oxalate Precipitation. Control Sample Z-1.

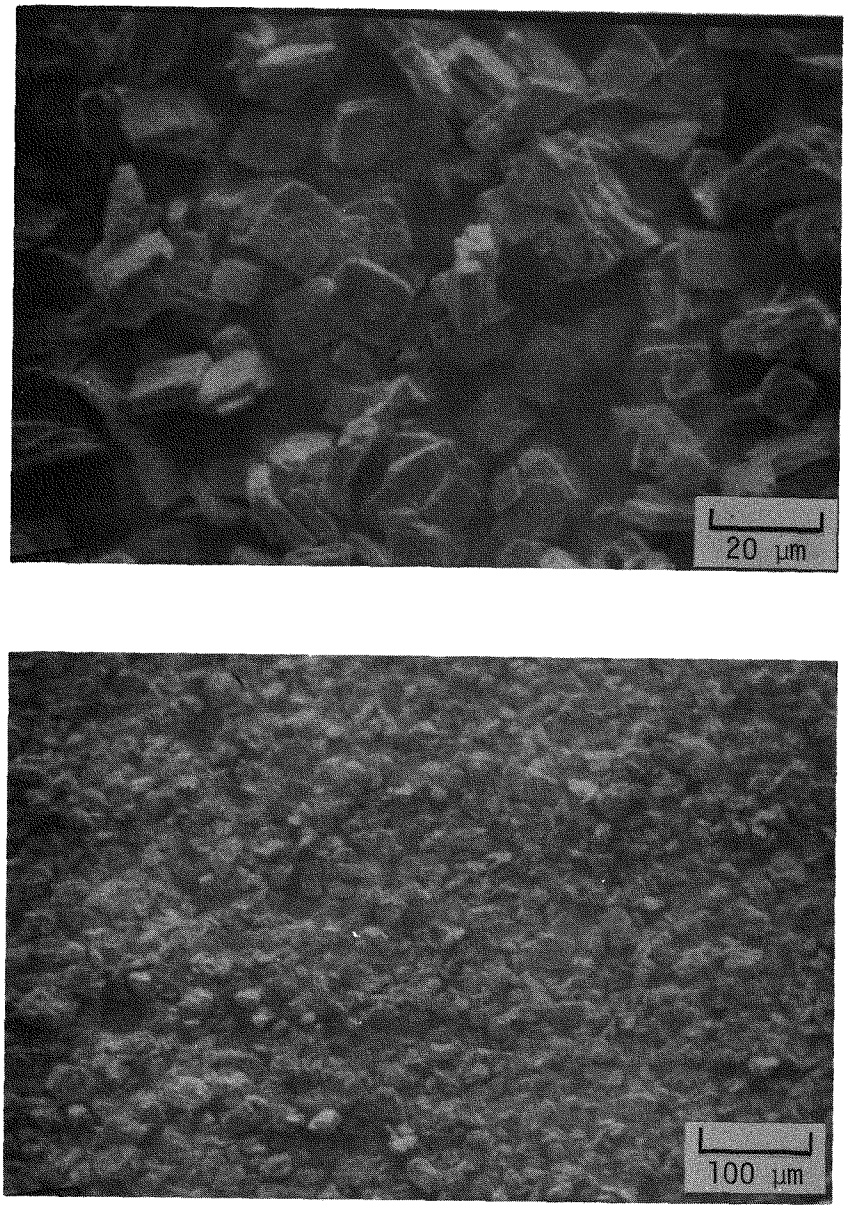

FIGURE 3. Effect of Heel on Morphology of $^{239}PuO_2$ Produced by Pu(IV) Oxalate Precipitation. Sample Z-2.

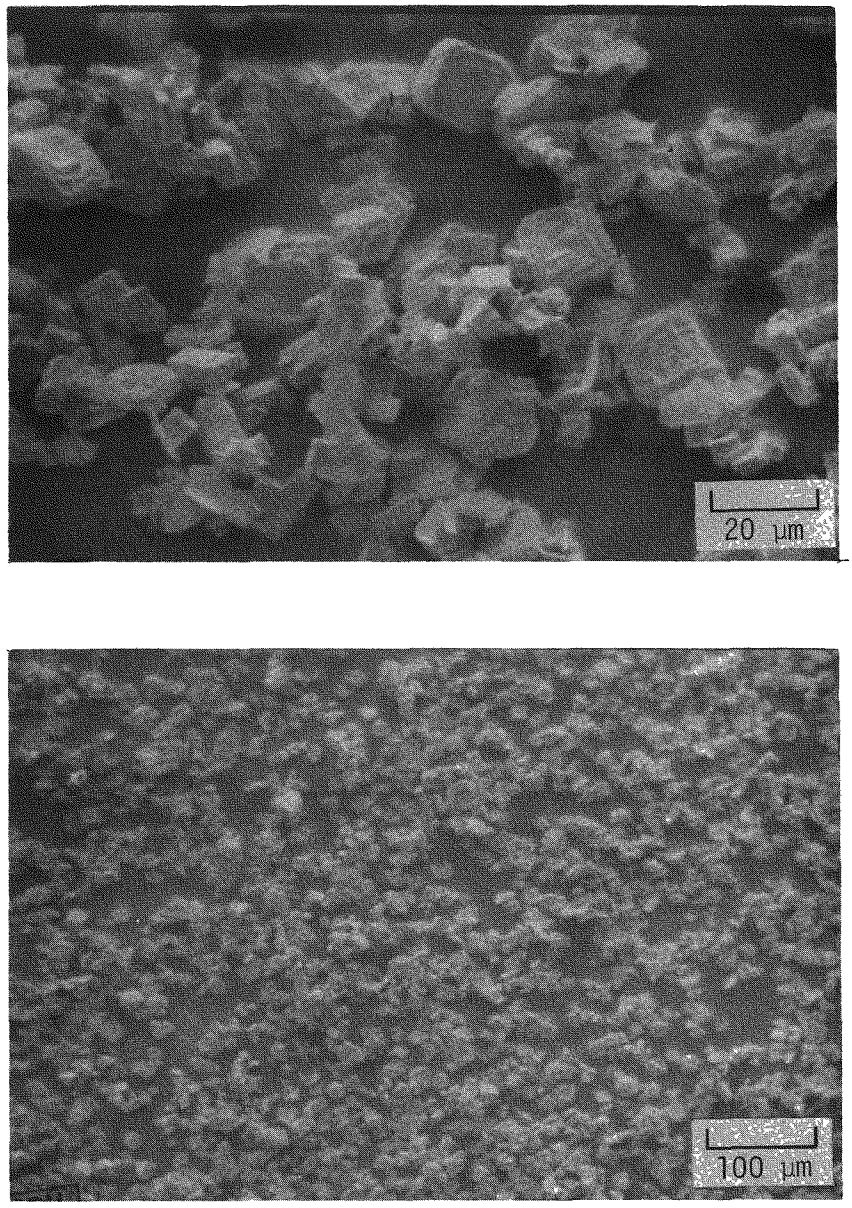

FIGURE 4. $^{238}PuO_2$ Produced by Pu(IV) Oxalate Precipitation. Sample P-1. $^{238}PuO_2$ versus $^{239}PuO_2$

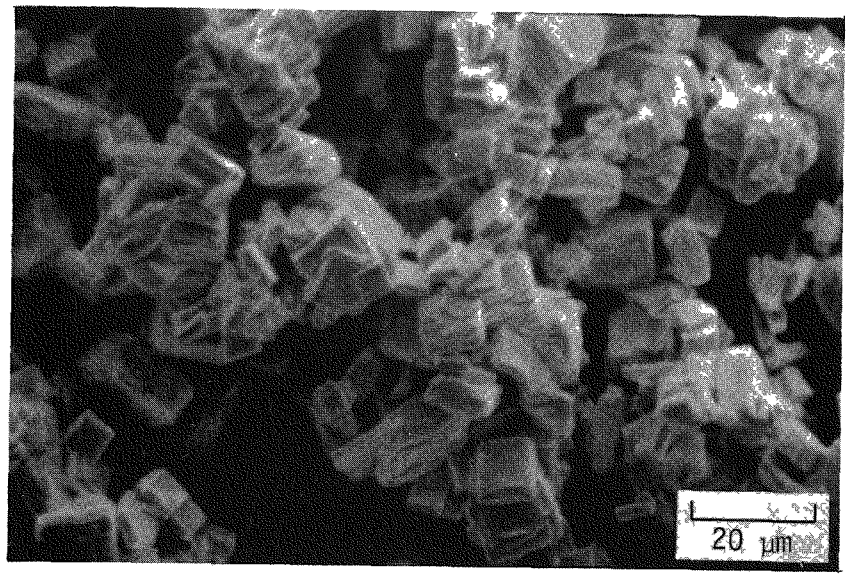

Sample P-1

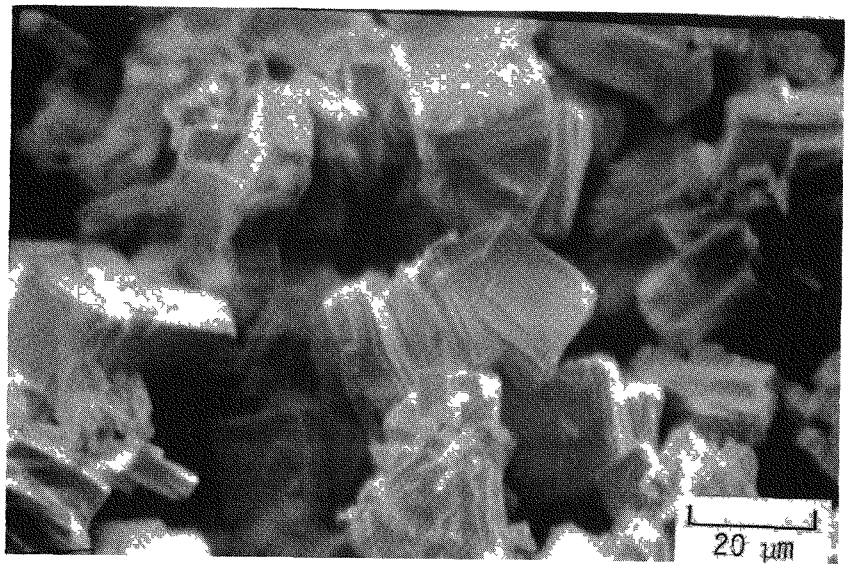

Sample T-1C

FIGURE 5. Interior of Small Aggregates of $^{238}PuO_2$ Produced in Laboratory Precipitation of Pu(IV) Oxalate. Sieved, +53 µm

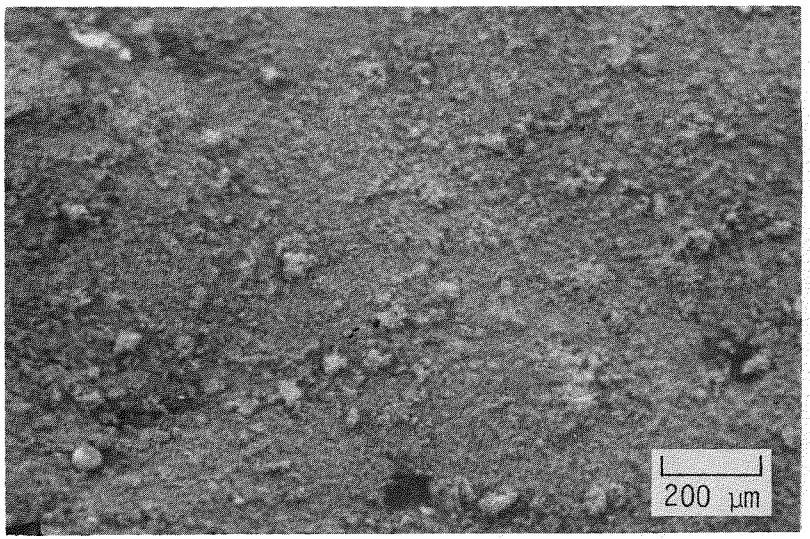

As Screened, -44 µm

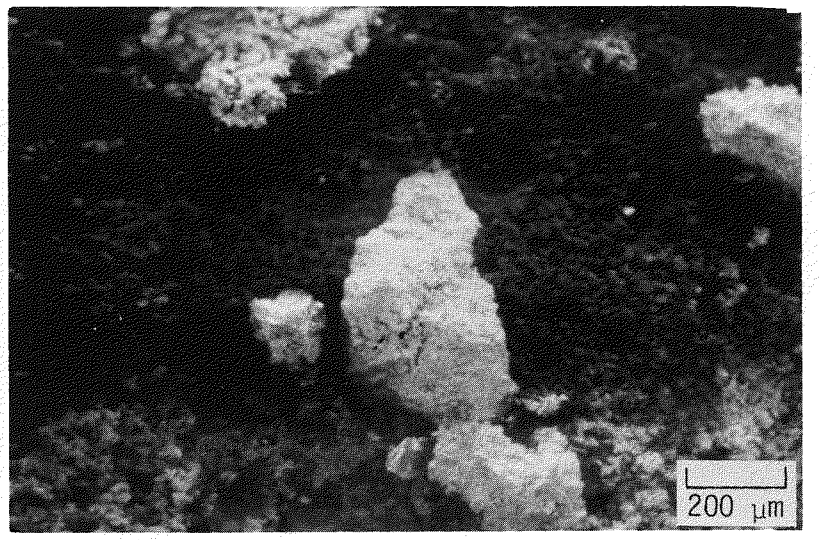

As Received

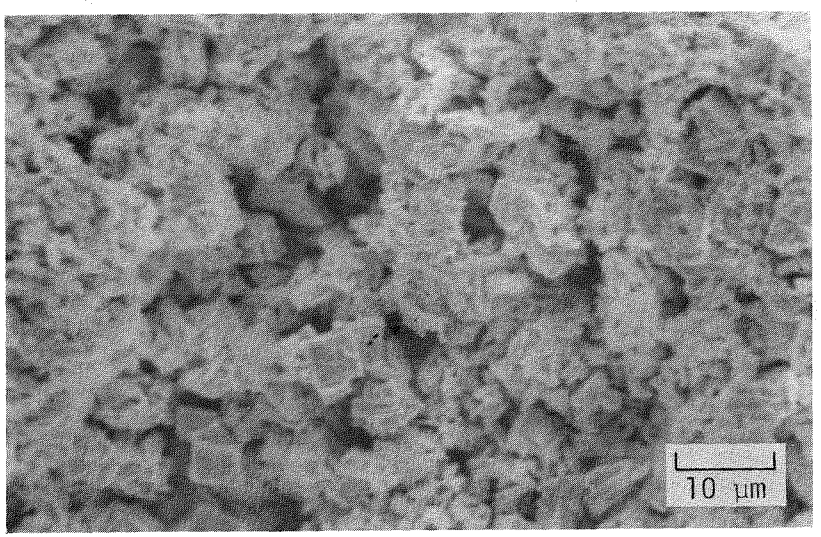

Interior of Agglomerate

FIGURE 6. $^{238}PuO_2$ Produced by Precipitation of Pu(IV) Oxalate in HB-Line. Sample HA 737.

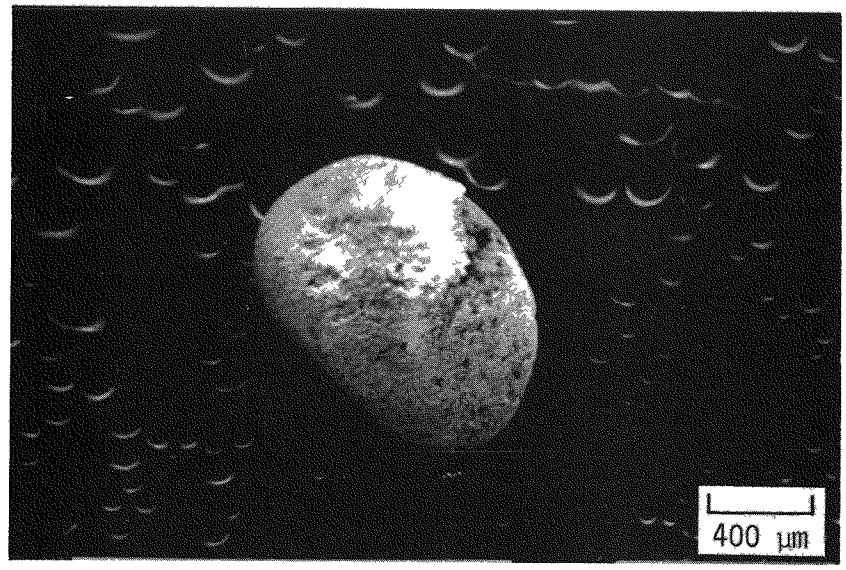

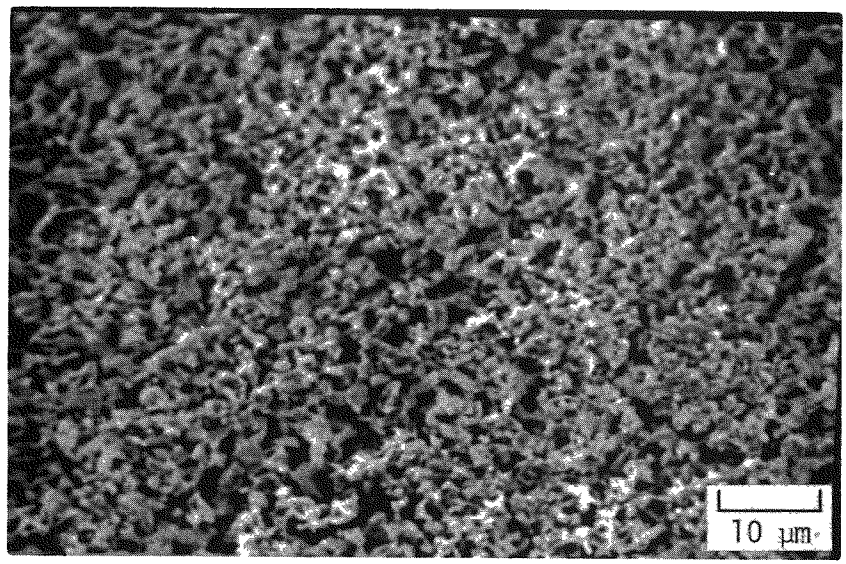

FIGURE 7. $^{238}PuO_2$ Produced by Precipitation of Pu(IV) Oxalate in HB-Line. Hand-plucked agglomerate from Sample HA 737.

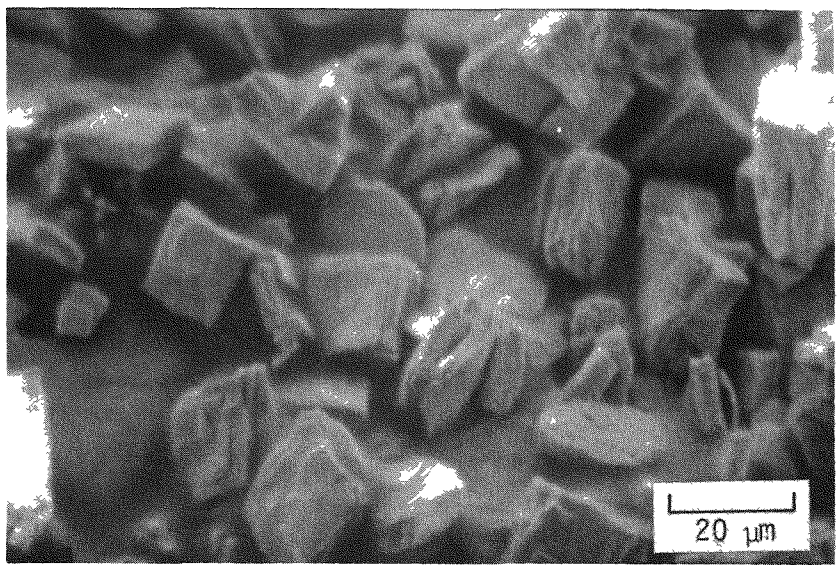

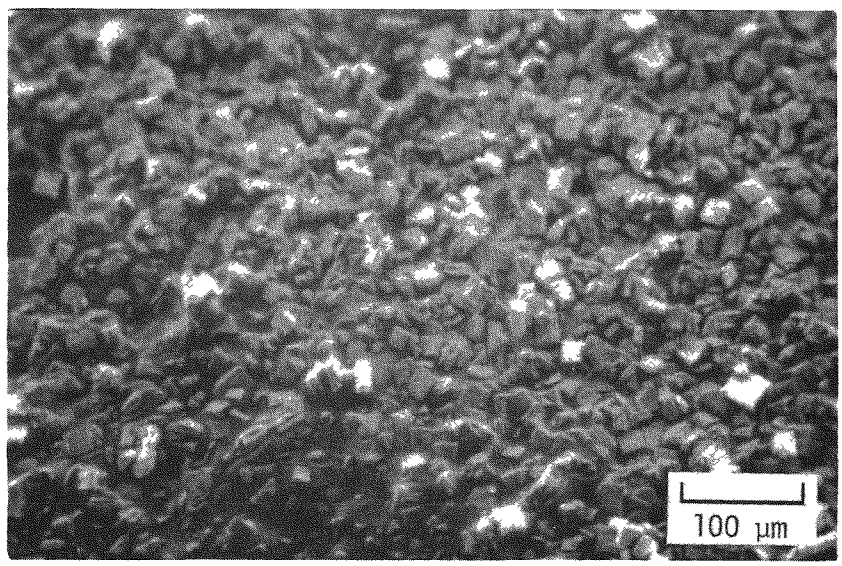

FIGURE 8. $^{239}PuO_2$ Produced by Precipitation of Pu(IV) Oxalate. No stirring during feed addition. Sample T-2M.

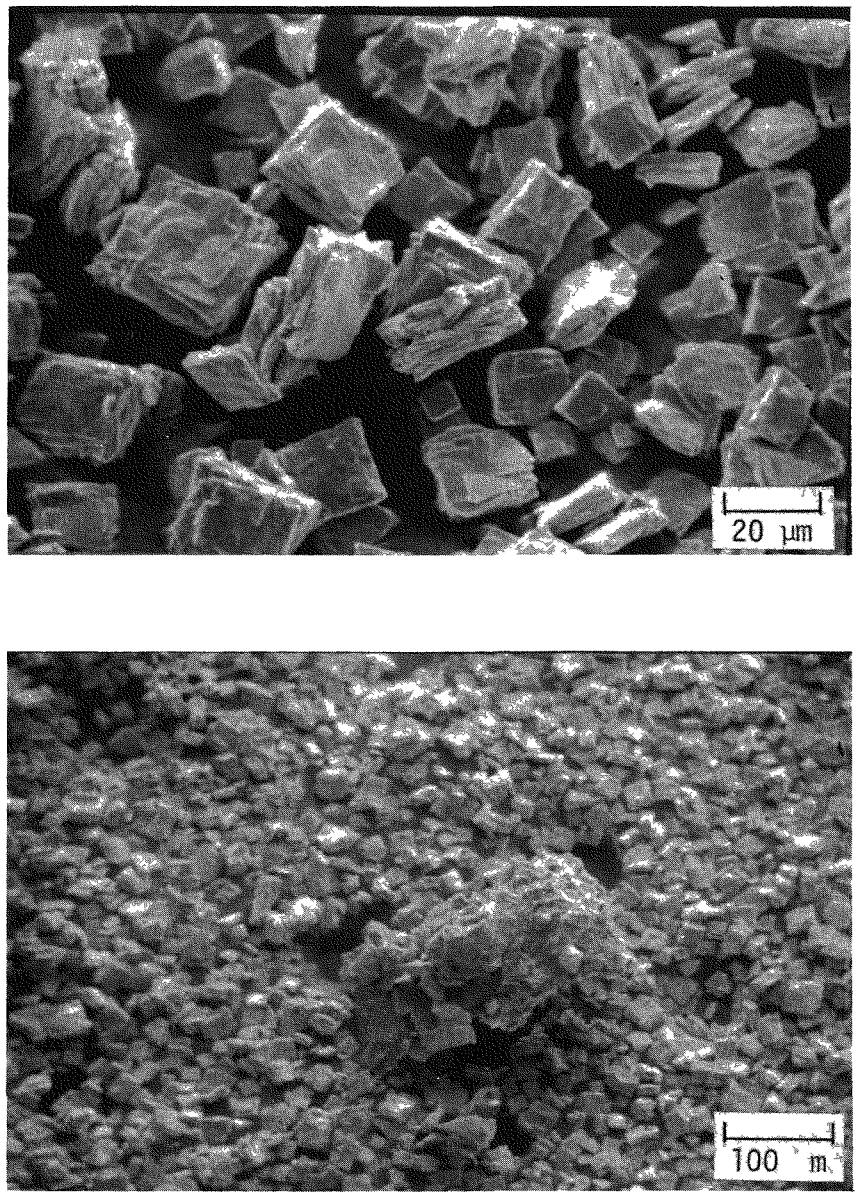

FIGURE 9. $^{239}PuO_2$ Produced by Precipitation of Pu(IV) Oxalate. 150-rpm stirring during feed addition Sample T-2D.

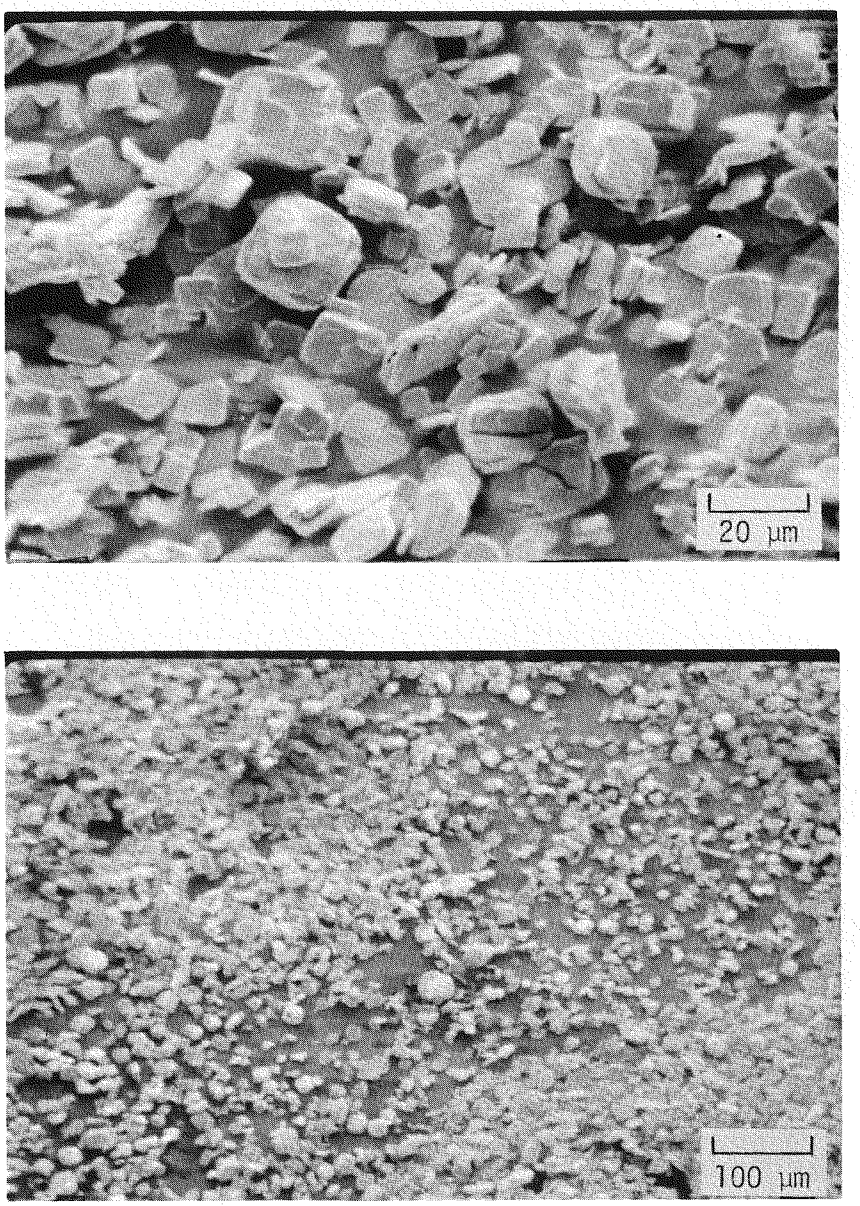

FIGURE 10. $^{239}PuO_2$ Produced by Precipitation of Pu(IV) Oxalate. 900-rpm stirring during feed addition. Sample T-2E.

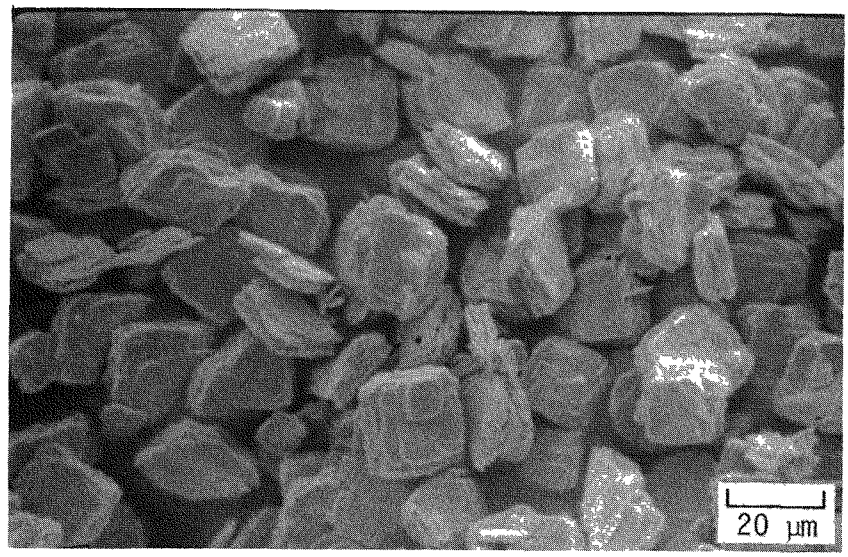

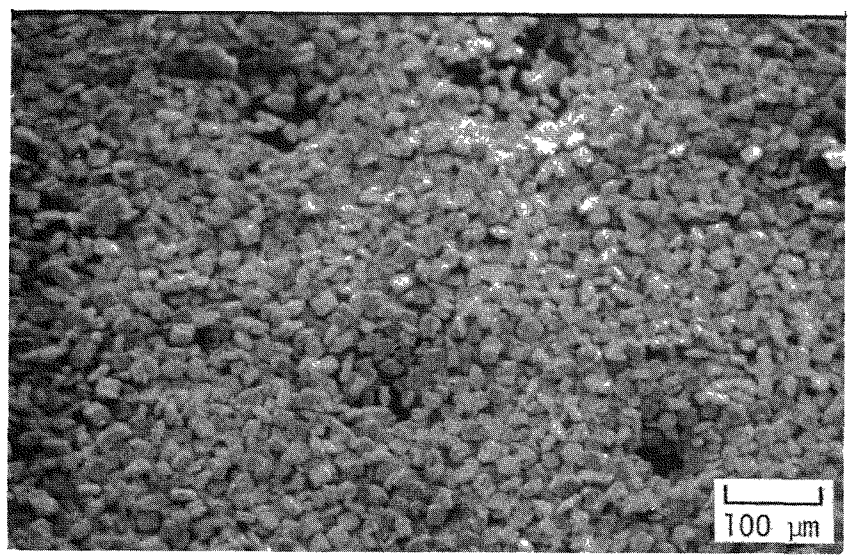

FIGURE 11. $^{239}PuO_2$ Produced by Precipitation of Pu(IV) Oxalate. High Pu concentration in feed. Sample T-2F.

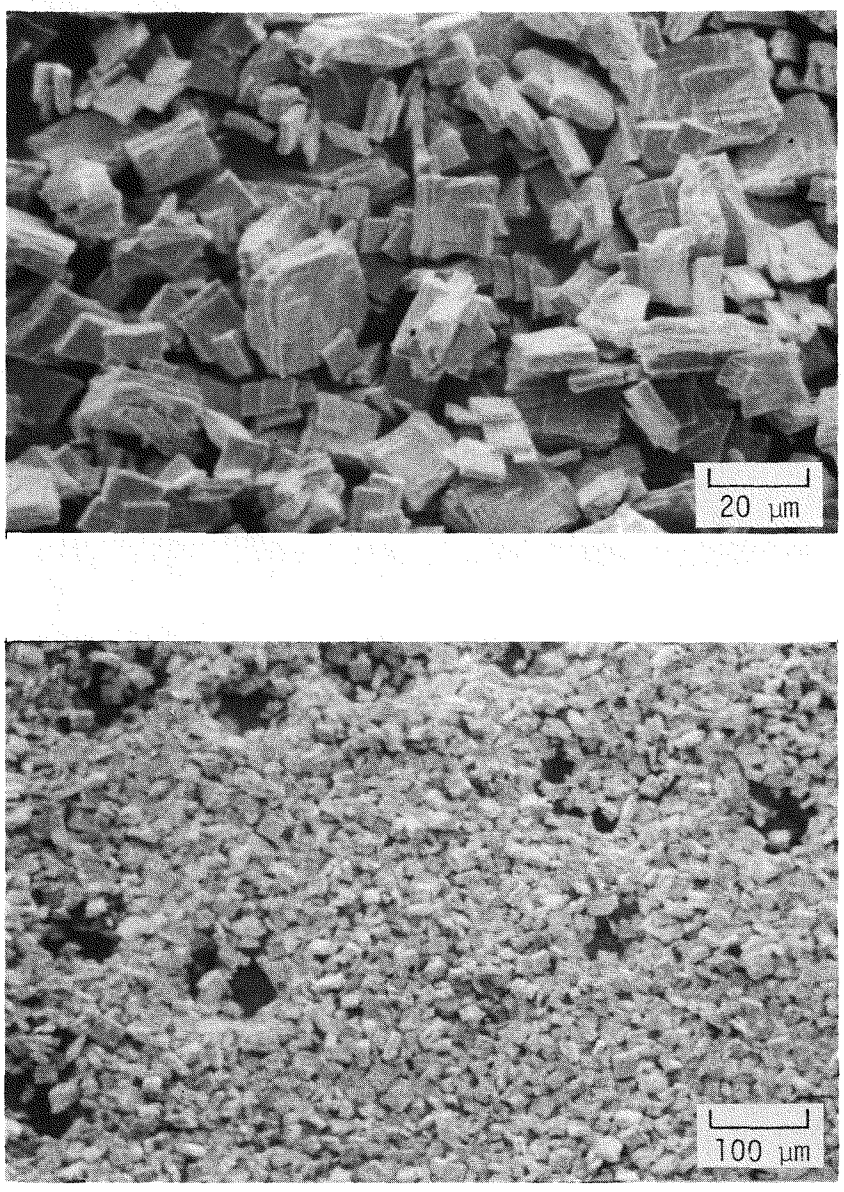

FIGURE 12. $^{239}PuO_2$ Produced by Precipitation of Pu(IV) Oxalate. High HNO_3 concentration in feed. Sample T-2G.

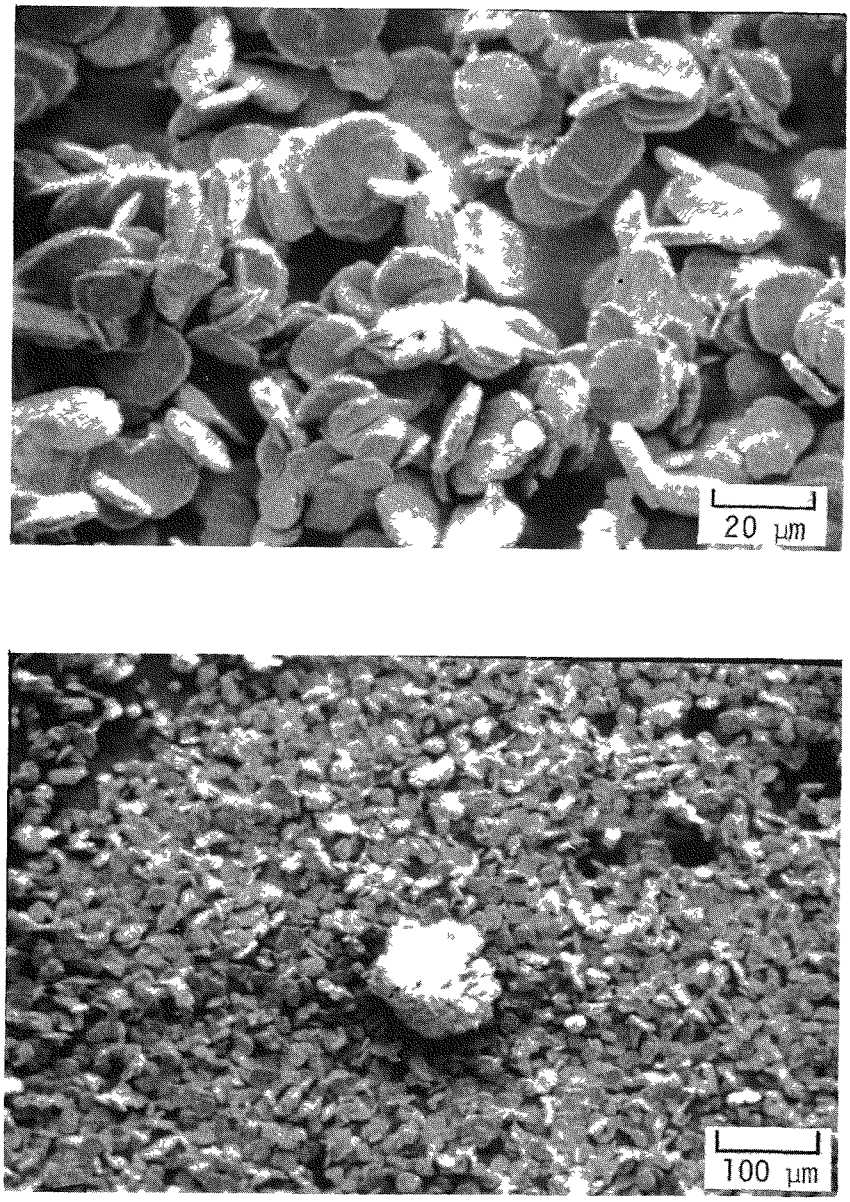

FIGURE 13. $^{239}PuO_2$ Produced by Precipitation of Pu(IV) Oxalate. Low HNO_3 concentration in feed. Sample T-2H.

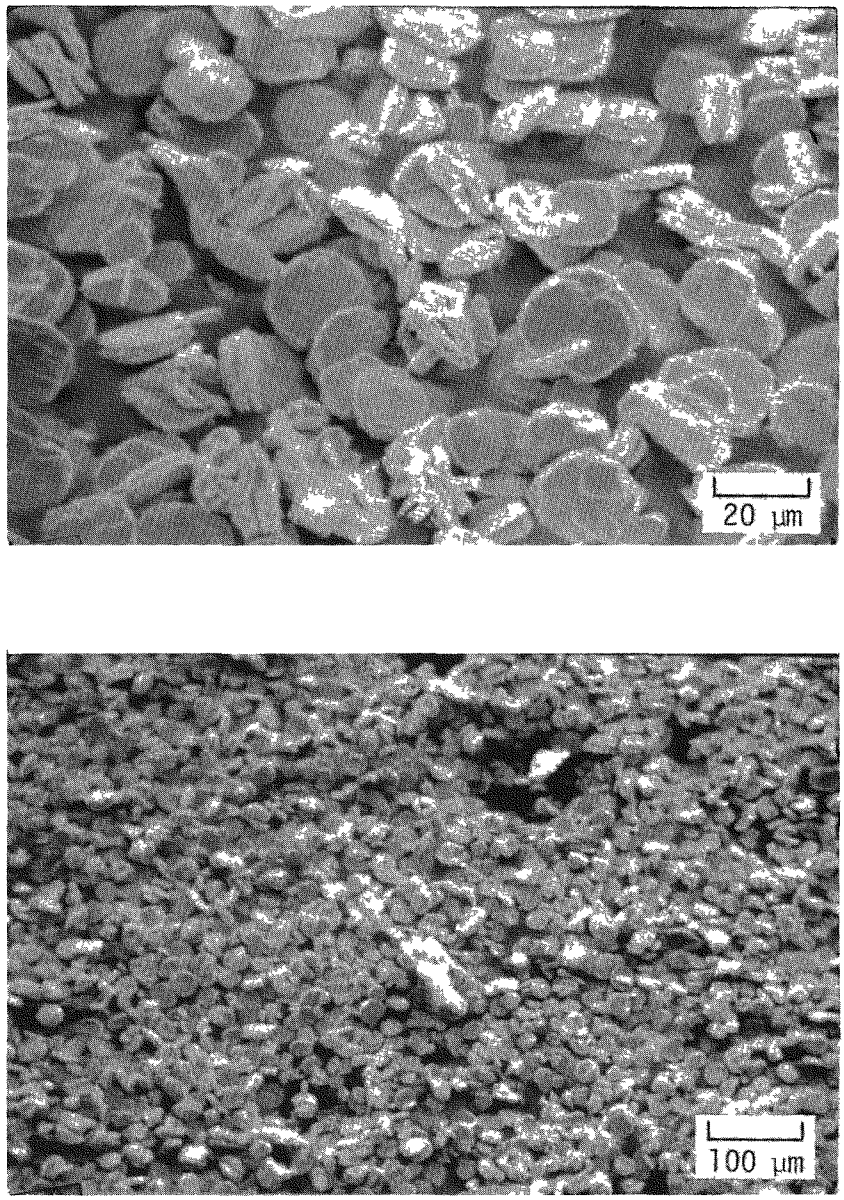

FIGURE 14. $^{239}PuO_2$ Produced by Precipitation of Pu(IV) Oxalate. Up-down temperature variation. Sample T-2K.

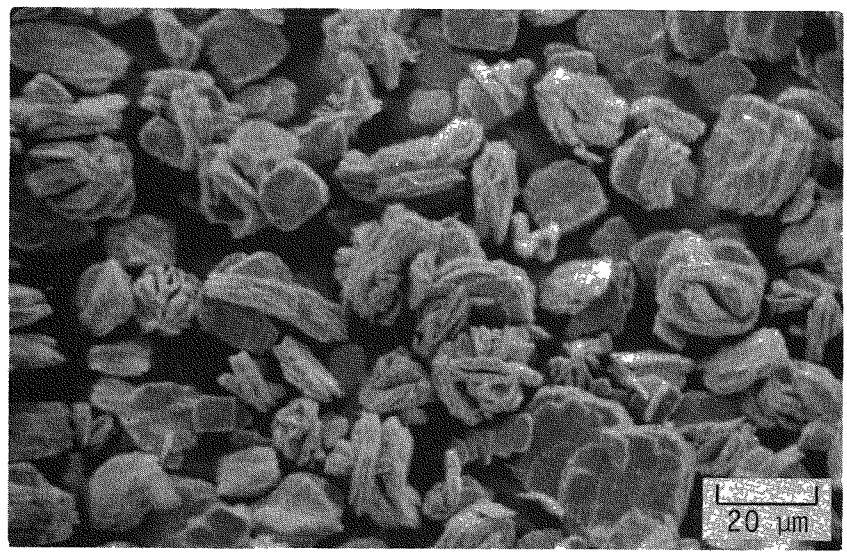

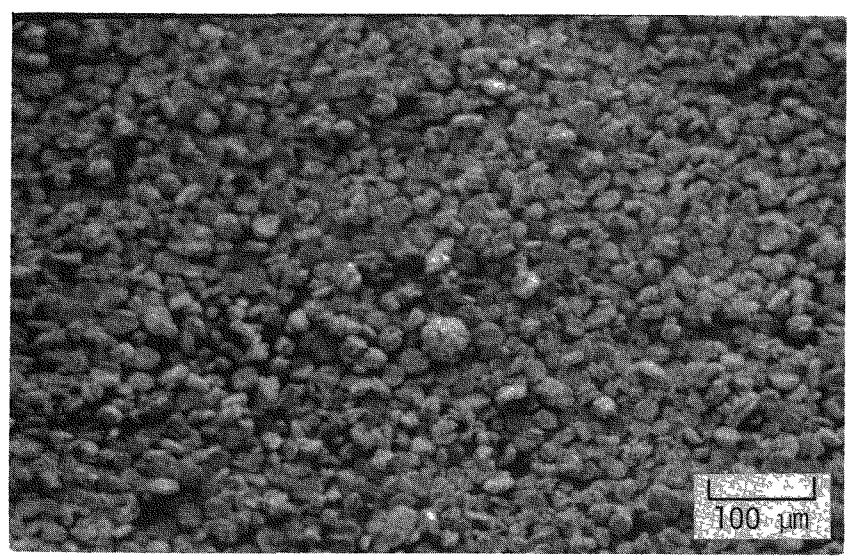

FIGURE 15. $^{239}PuO_2$ Produced by Precipitation of Pu(IV) Oxalate. Down-up temperature variation. Sample T-2L.

Residual "Heel" in the Precipitator

Residual plutonium oxalate crystals (the "heel") in the bottom of the precipitator vessel from previous precipitation runs had no effect on the size distribution or morphology of calcined PuO_2. It was postulated that residual seed crystals might promote excessive or premature nucleation during the addition of Pu nitrate solution to the oxalic acid. Pu(IV) oxalate precipitation does not begin immediately with the first feed added. About two-thirds of the Pu and its nitric acid complement must be admixed before the solubility limit of the oxalate complex is exceeded and precipitation begins. As shown in Table 1 and Figures 1-3 for ^{239}Pu samples Z-1 and Z-2, there is no significant difference in the powders obtained with and without seed crystals. The normal and desired powder of unagglomerated, rectangular prisms with a unimodal size distribution was obtained in both the control and seeded precipitations.

^{238}Pu Versus ^{239}Pu

Some tendency towards diminutive particles and aggregation was observed when ^{238}Pu(IV) oxalate obtained from HB-Line feed solution was precipitated rather than ^{239}Pu. However, the size and morphology of this powder are significantly improved over powder from plant precipitations, and the powder properties appear to be satisfactory for fabrication.

^{238}Pu sample P-1 (Table 1) was precipitated in laboratory equipment from a different batch of HB-Line Pu nitrate than was used to produce the 1200 g of low-quality $^{238}PuO_2$ last fall. Both the particle size distribution (Figure 1) and photomicrographs of Figure 4 show that the rectangular prisms are slightly smaller than in powder from the other laboratory precipitations, 8 to 13 μm mode size compared to 15 to 20 μm. The slight tendency to form smaller particles in Sample P-1 was not observed in previous laboratory-scale precipitations of ^{238}Pu using feed that had been prepared from dissolved B-Line $^{238}PuO_2$ and purified in laboratory ion exchange columns rather than in plant equipment (Samples T-1A, T-1B, T-1C and T-1D of the October 1976 and March 1977 monthly reports.)[4,5]

The smaller prismatic particles in Sample P-1 showed a tendency for aggregation, but, in contrast to lant precipitations, no agglomerates containing nondescript micron-sized particles were observed (Figure 5). Sieving sample P-1 and Sample T-1C from an earlier laboratory ^{238}Pu(IV) precipitation[5]

through a 53-μm screen produced ≤5 vol % of agglomerates or aggregates of <500 μm compared to 50 vol % of agglomerates of ≤¼ inch for production powder.

These large agglomerates in the HB-Line feed caused the inhomogeneous microstructure in test pellets described in the March-April 1978 report.[1] Further, the excess shrinkage (increase of 4 to 5% TD) observed on heat treating pellets hot pressed from HB-Line feed in subsequent fabrication tests can be attributed to the small (∿1 μm) nondescript particles comprising these agglomerates.

The large differences in the characteristics of the agglomerates in HB-Line feed powder compared to powder made in laboratory precipitations of plant feed solution are shown in Figures 5, 6, and 7. The friable agglomerates in the HB-Line feed (Figure 6) are irregularly shaped and contain occluded small prisms. These agglomerates broke up readily when rolled through a 44-μm screen to obtain a more free-flowing powder. However, some agglomerates in the HB-Line product were sufficiently strong to permit handling with tweezers. These agglomerates appear as smooth globules which are comprised entirely of nondescript, micron-size particles (Figure 7) which cause excess shrinkage in pellets.

The greater radiation from ^{238}Pu over ^{239}Pu might be expected to cause differences in particle size and morphology between precipitations of ^{238}Pu and ^{239}Pu oxalate. Microscopic bubbles of radiolytically formed gases might promote excess nucleation or interfere with precipitation kinetics by affecting the transport of precipitating ions through the methorical layer around growing crystals. However, radiolysis does not appear to be the major cause of the precipitation problem in HB-Line, because the laboratory precipitations using ^{238}Pu feed solution from HB-Line did not radically change the characteristics of PuO_2 as had occurred in the plant. The 60-g scale of the plant precipitations does not produce a higher rate of radiation damage per volume of slurry than that which occurs in the 1-g laboratory precipitations because the Pu concentrations and times were the same.

Because acceptable ^{238}Pu feed can be obtained in the laboratory, and different plant feed stock apparently causes different powder characteristics, the problem in the plant is probably related to equipment or chemistry and, hence, is correctable. One hypothesis that will be evaluated is that excess nucleation is caused by the presence of submicron fragments of heavily degraded ion exchange resin in HB-Line feed solution. The occasional presence of agglomerates and aggregates of nondescript submicron particles in the usual plant feed made from Pu(III) oxalate also may be associated with resin fragments (p. 16 of the February 1976 report).[6]

Stirring Rate During Precipitation

Size and morphology data on Samples T-2M, T-2D, and T-2E (Table 1) show that variations in stirring rate during feed addition and digestion do not cause agglomeration or fine particles. A free-flowing powder consisting only of the rectangular prisms was obtained with no agitation and with stirring at 150 rpm and 900 rpm. Although the stirring speed in the plant precipitator varies along the radius of the larger paddles and could not be duplicated in these laboratory tests, the stirring rates in the tests spanned the speed range in plant equipment.

Some second-order effects on particle size, distribution, and morphology were observed. Suprisingly, the size distribution and shape of the rectangular prisms were normal even with no stirring, demonstrating the propensity for self nucleation (Figures 1 and 8) Agitation at what is believed to be a more typical rate for plant equipment (150 rpm) also produced normal particles (Figure 9) with some tendency towards larger prisms (Figure 1). Very rapid stirring at 900 rpm tended to produce smaller (Figure 1), but still well-formed prisms (Figure 10).

High Pu Concentration in Feed

A high Pu concentration in the nitrate feed solution (10 g Pu/L vs. 4 to 6 g Pu/L) produced no agglomerates or fine particles (Sample T-2F in Table 1). In fact, this powder had the thickest and best-developed prisms and appeared to be the freest-flowing powder of all tests to date (Figures 1 and 11). Such a powder should have the best fabrication response of any of the powders observed to date. The higher Pu concentration in the feed may also increase the throughput in HB-Line.

Nitric Acid Concentration in the Feed

Neither high (2.2M) nor low (0.5M) nitric acid concentration in the feed caused agglomeration or nondescript micron-sized particles (Samples T-2G and T-2H of Table 1 and Figure 1). High acid concentration showed some tendency to cause smaller prisms (Figure 12). Low acid concentration caused some rounding of the corners of the prisms (Figure 13). These powders retained desirable fabrication properties even though the acid concentrations were varied to limits where the characteristics of powder from Pu(III) precipitations would be unacceptable.

Precipitation Temperature

Varying temperature during feed addition had little effect on the tendency to form agglomerates and nondescript micron-sized particles. The oxalate solution temperature varies a few degrees as warm ^{238}Pu nitrate feed solution is added to oxalic acid because cooling by the water jacket on the plant precipitator cannot maintain precise temperature control. The approximate sine-wave variation of temperature of 6 to 10°C in the production test last year was postulated as a likely cause of varying precipitation kinetics.[3] However, in laboratory precipitations (Samples T-2K and T-2L) half-sine-wave variations of temperature, whether increasing 6 or decreasing 7°C, did not produce the undesirable sizes and morphologies observed in plant-produced powder (Table 1 and Figure 1). As shown in Figures 14 and 15, there was some tendency to form prisms with rounded corners and to form small (10 to 20-μm) aggregates, neither of which is expected to compromise fabricability.

Program

Larger-scale (15-g) ^{238}Pu precipitations will be performed in laboratory equipment to test scale effects on ^{238}Pu oxalate. Variations in powder characteristics will be evaluated for different feed lots precipitated in HB-Line and correlated with the age of the resin in the last ion exchange column in the plant. Inferior $^{238}PuO_2$ produced in the plant will be dissolved and reprecipitated to eliminate any degraded-resin effects. Concurrently, fabrication tests are proceeding to find the conditions to produce satisfactory pellets and spheres from the presently inferior HB-Line feed.

MICROSTRUCTURAL DAMAGE PRODUCED BY HELIUM IN 95%-DENSE COLD-PRESSED-AND-SINTERED $^{238}PuO_2$ PELLETS

Heating of 95%-dense, cold-pressed-and-sintered $^{238}PuO_2$ pellets after 14 months' aging produced large internal cracks attributed to agglomeration of decay helium. The large cracks were formed above 1200°C by interlinking of grain-boundary separations in the small-grained microstructure. Lower-density forms with sufficient interconnected porosity to release decay helium will be needed to avoid such microstructural damage in cold-pressed-and-sintered $^{238}PuO_2$.

The specimens examined were segments of two cold-pressed pellets prepared originally to establish effects of pre-sintering temperature on granule density (April 1976 Report[7], p. 20) and later sintered to determine their susceptibility to

internal cracking (March 1977 report[5], p. 7). The pellets (CP-84 and -89) had been formed by cold-pressing milled $^{238}PuO_2$ powders (1.75-μm mode) at 58,000 psi and presintering at temperatures of 1050 and 1300°C, respectively; final sintering for 5½ hr at 1350°C produced densities of 94 and 95% TD, respectively. Metallographic examination of the as-sintered pellets showed small rounded pores within and on the grain boundaries of a generally well-consolidated, small-grained (5 to 7-μm) microstructure. Lower-density regions observed occasionally exhibited smaller grains surrounded by large grain-boundary pores.

After storage near room temperature for 14 mo, two segments of the pellets were heated for 3 hr at 1200 and 1400°C, respectively, and examined metallographically for comparison with an unheated specimen. The unheated specimen exhibited a small-grained microstructure with porosity distribution analogous to the as-sintered specimen; low-density areas persisted, but no general grain separation or cracking of the specimen was evident (Figure 16). Conversely, the specimens heated at 1200°C and 1400°C exhibited pronounced grain separations and related cracking. In the specimen heated at 1200°C, the microstructure was dominated by grain-boundary bubbles and separations, although some areas free of microstructural damage were observed (Figure 17). No pronounced cracking was observed. In the specimen heated at 1400°C, the grain separations were less severe, but many large cracks were formed apparently by interlinking of grain separations (Figure 18).

Both the grain separations and the large cracks are attributed to agglomerations of decay helium at high temperatures in the aged specimens. At 1200°C, near the temperature threshold for microstructural damage, the agglomerated helium produced predominantly localized grain separations. At 1400°C, the helium, unable to escape the high-density pellet, collected into large cracks in the structure. Release of the helium into the large cracks at 1400°C prevented to some extent the more localized damage produced at 1200°C.

To avoid such microstructural effects of helium in cold-pressed-and-sintered $^{238}PuO_2$, lower-density forms with interconnected pores are required to allow helium release without crack formation. Cold-pressed-and-sintered forms with densities as low as 85% TD, as prepared directly from coarse feed particles obtained by calcination of reverse strike Pu(IV) oxalate precipitates (March-April 1978 Report[1]), might be suitable.

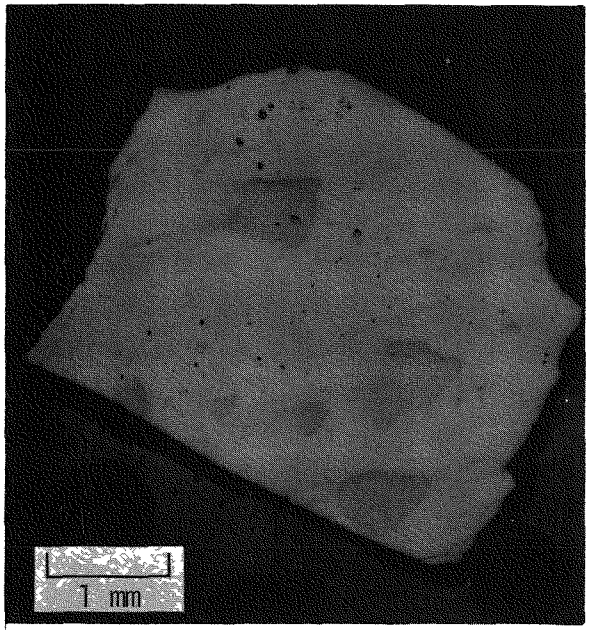

a. Etched 1/2 hr

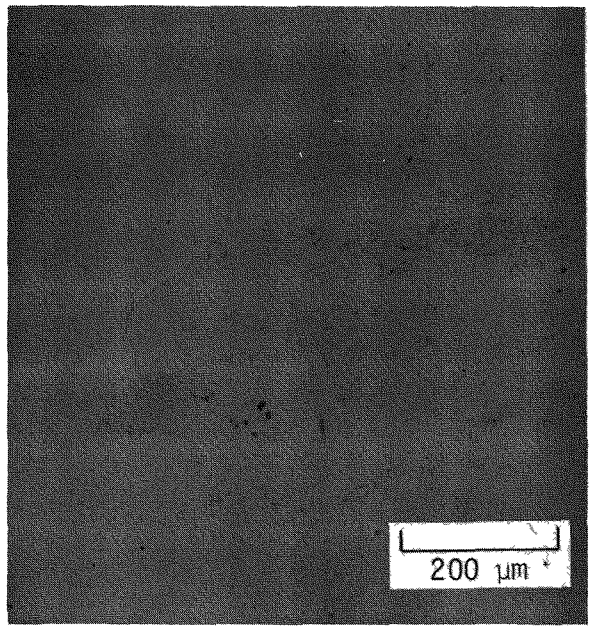

b. Etched 1/2 hr

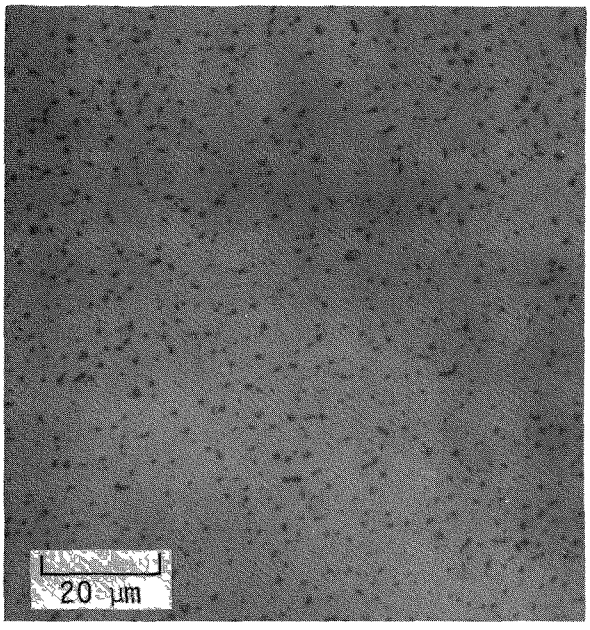

c. Etched 1/2 hr

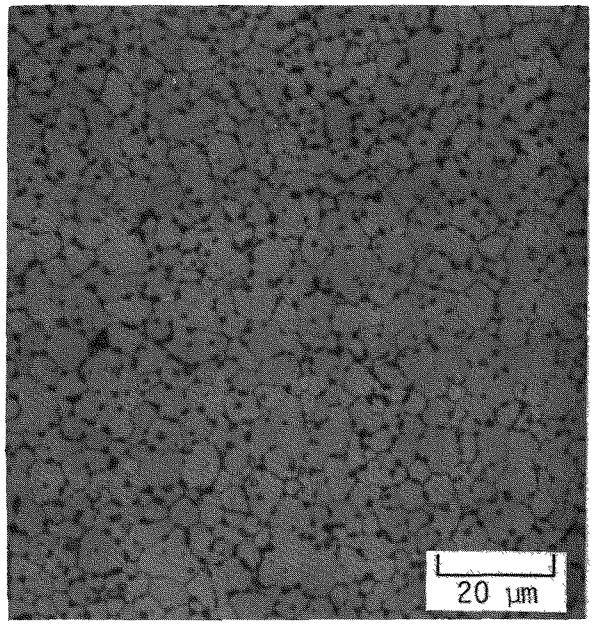

d. Etched 3-1/2 hr

FIGURE 16. Microstructures of Cold-Pressed-and-Sintered $^{238}PuO_2$. Pellet CP-84 after 14-months aging. No heat treatment. Dark spots in (a.) are low-density regions.

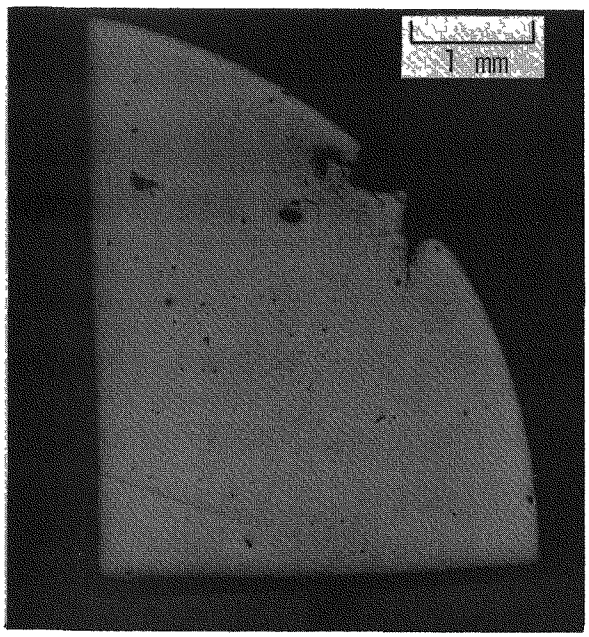

a. Etched 1/2 hr

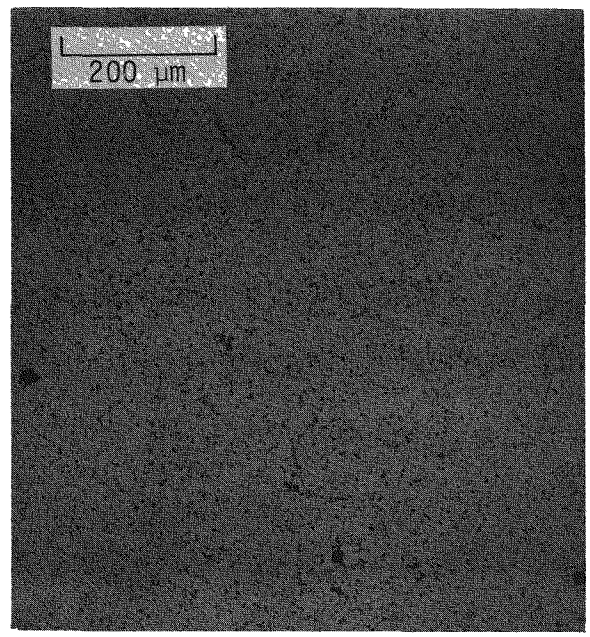

b. Etched 1/2 hr

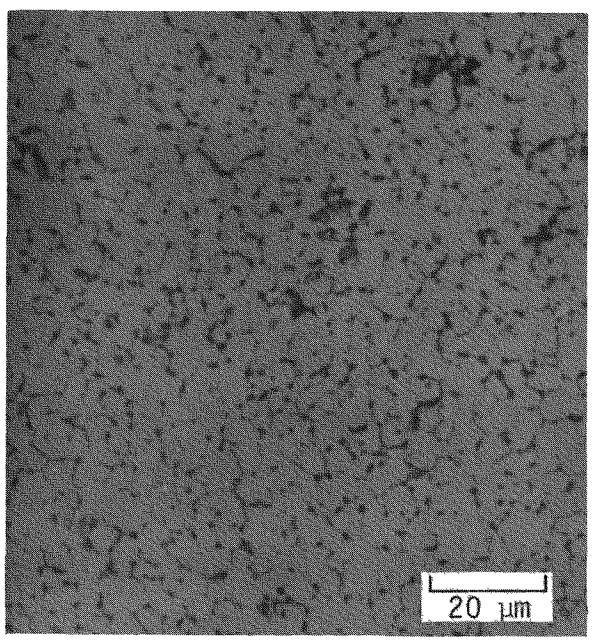

c. Etched 1/2 hr

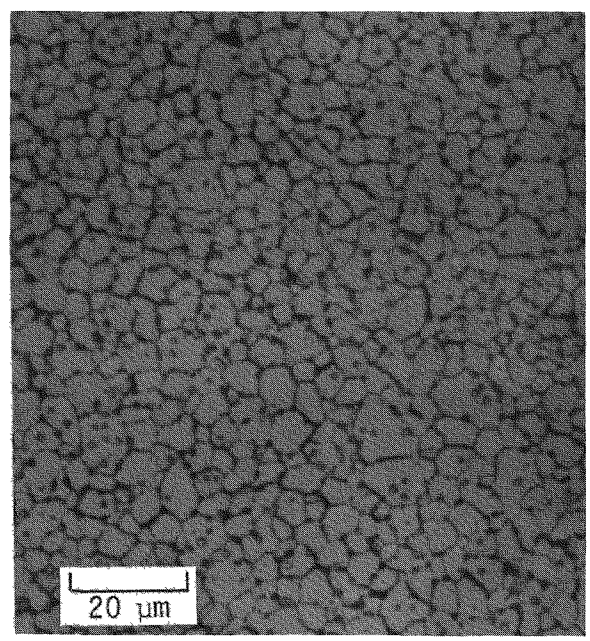

d. Etched 7 hr

FIGURE 17. Microstructures of Cold-Pressed-and-Sintered $^{238}PuO_2$ Pellet CP-89 after 14-mo Aging and Heating 3 hr at 1200°C

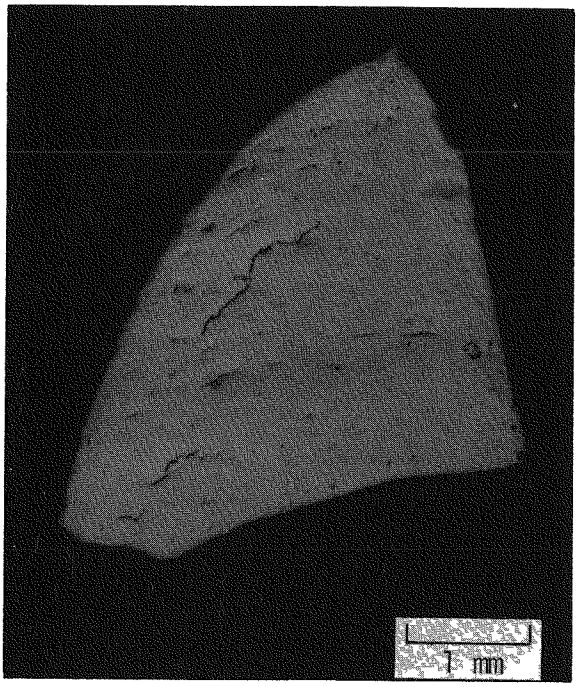

a. Etched 1/2 hr

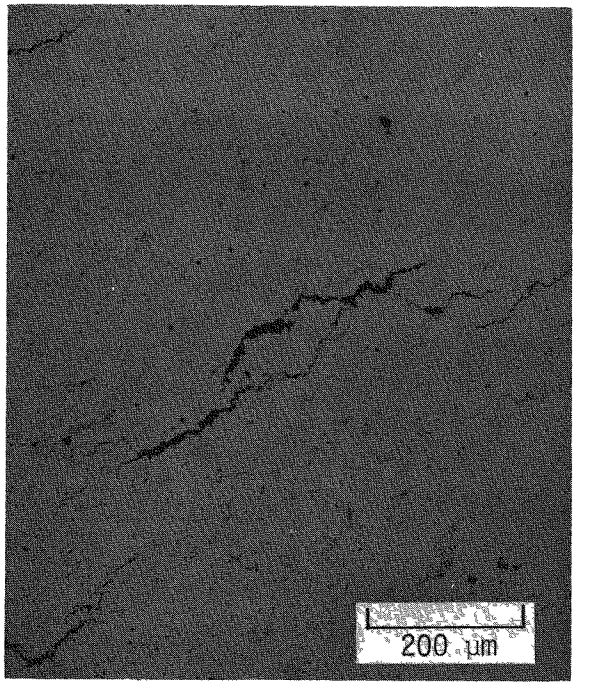

b. Etched 1/2 hr

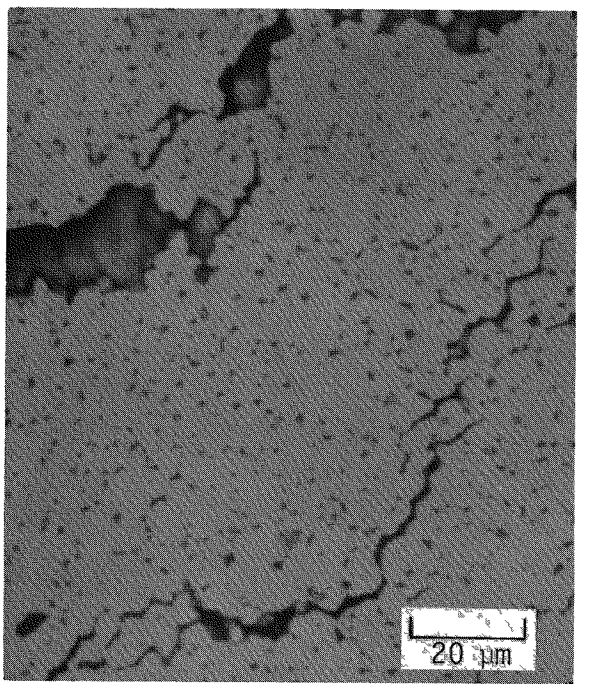

c. Etched 1/2 hr

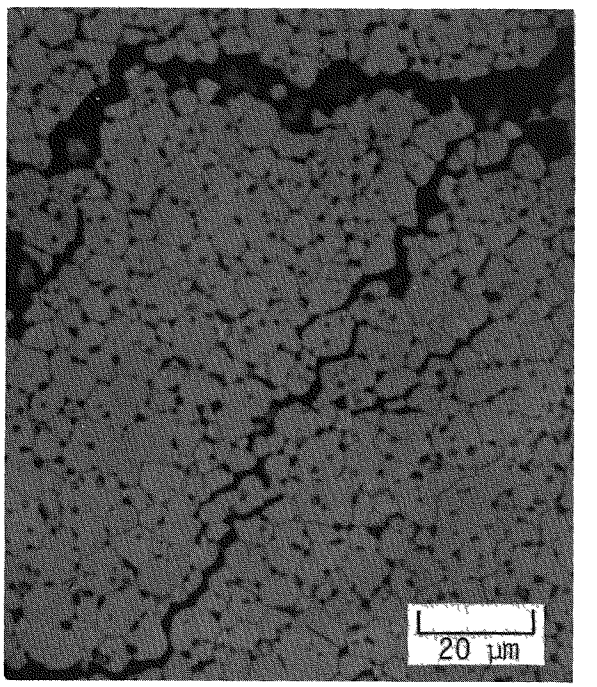

d. Etched 5 hr

FIGURE 18. Microstructures of Cold-Pressed-and-Sintered $^{238}PuO_2$ Pellet CP-84 after 14-mo Aging and Heating 3 hr at 1400°C.

MILLIWATT PROCESS DEVELOPMENT

FABRICATION OF OXALATE-BASED SHARDS

A proof test program for fabricating prototypic $^{238}PuO_2$ shard fuel for Milliwatt (MC 2893) Heat Sources was initiated to demonstrate the comparability of high-fired PuO_2 shards made from calcined Pu oxalate feed powder (SRL process) to shards made from hydroxide feed (existing Mound Facility production process). Part I of the program was to demonstrate the proposed oxalate-based flowsheet (October 1977 report[8] Figure 19) on a laboratory-scale in the AMF. Part II of the program was to use this flowsheet to produce ∿150 g of Milliwatt shards in the PuFF and PEF for tests at MF to determine the chemical compatibility of the shards and T-III liner and the quantity of fines generated on impact.

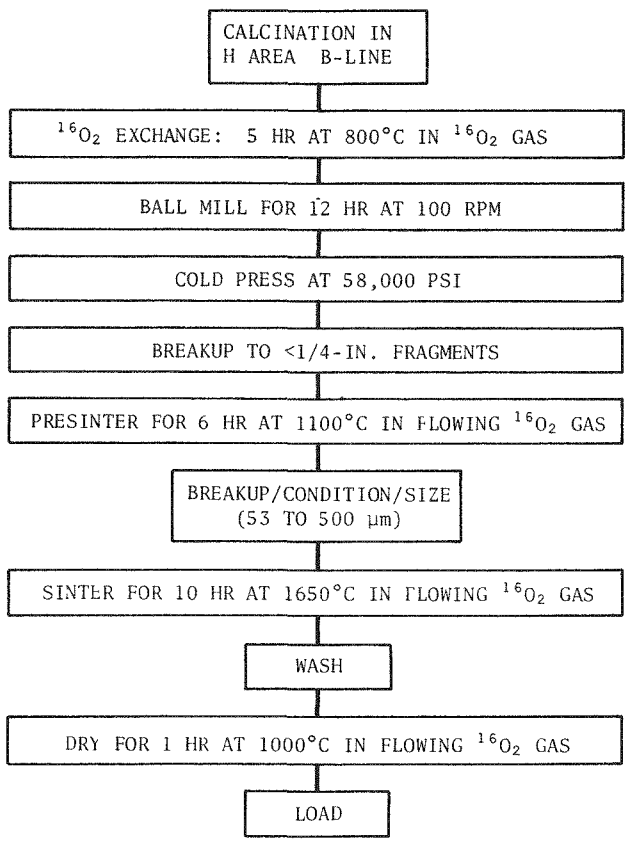

FIGURE 19. Flowsheet for Milliwatt Shard Production

The laboratory-scale fabrication test in the AMF successfully demonstrated that the current SRL flowsheet can produce acceptable shards for Milliwatt Heat Sources. However, shards made in the production-scale fabrication test in PuFF/PEF had marginal characteristics (morphology, size and fines) apparently resulting from a scaleup problem associated with the cold-pressing and sizing steps. Unlike shards in previous batches, these shards possessed surface asperities which could fracture on impact and generate more fines than would be expected from shards made in the AMF tests. About 180 g of these marginal shards were shipped to MF for testing.

A development program to correct the scaleup problem in cold pressing and sizing and to optimize the process for production has been cancelled because of the recent transfer of Milliwatt fuel production to LASL. No further work on Milliwatt fuel at SRL is planned.

Flowsheet Demonstration in AMF

Two ∿70-g batches of shards were made in the AMF according to the flowsheet of Figure 19 to demonstrate the acceptability of shards made by the SRL oxalate-based process. These shards, the first produced according to the proposed flowsheet, had properties comparable to hydroxide-based shards produced at MF (Table 2). The flowsheet of Figure 19, described in the October 1977 report[8], evolved from a series of fabrication experiments in 1975 (August 1975 report[9]). The batch sizes of PuO_2 associated with each process step in the AMF test and the subsequent full-scale test in PuFF/PEF are given in Table 3.

TABLE 2

Comparison of Physical Characteristics of Oxalate-Based Shards and Hydroxide-Based Shards

	Oxalate		
	AMF	*PuFF/PEF*	*Hydroxide*
Final Tap Density, g/cc	6.4	6.55	∿5.5
Shard Internal Density, %TD	∿97	93	∿97
Average Grain Size, μm	∿30	30	∿30
Fines Content, wt % <5 μm	4.7×10^{-3}	7.3×10^{-3}	$2\text{-}4 \times 10^{-3}$
Fines Content, wt % 5 to 10 μm	8.6×10^{-4}	5.1×10^{-3}	$4\text{-}6 \times 10^{-4}$

TABLE 3

Batch Sizes(grams) in Shard Fabrication Tests

Process Step	*AMF Test*	*Prototype Test*	
		PuFF	*PEF*
$^{16}O_2$ Exchange	70	150	
Ball Mill	70	75	
Cold Press	5	75	
Breakup	-	75	
Presinter	5	75	
Breakup/Condition/Size	5		75
Sinter	30		75
Wash	30		75
Dry	30		75
Load	-		

The shards made in the AMF test were analyzed for grain size and morphology, chemical purity, packing density and fines content. Results are summarized in Table 2 and briefly described below.

- *Morphology*. Examination by scanning electron microscopy (SEM) indicated the shards to be slightly acicular with a relatively smooth surface (Figure 20a). Absence of surface asperities should minimize generation of fines during subsequent handling and on impact. The average grain size was approximately 30 μm, which is comparable to MF shards.

- *Chemical Impurities* were determined by spark source mass spectroscopy. All elements with the exception of aluminum and silicon were within specifications (Table 4). Both aluminum and silicon are believed to have been introduced during sintering steps as a result of sluffing of old furnace refractory material, and should not be a problem in newer production

- *Packing Density*. The shards had a packing density of 6.4 g/cm^3 and thus can be readily loaded to the desired power density without vibrating. Normal packing density of hydroxide-based shards is about 5.5 g/cm^3.

- *Fines Content* determined by the MF washing and screening procedure was 8.6×10^{-4} wt % for particles 5 to 10 μm in diameter and 4.7×10^{-3} wt % for particles less than 5 μm in diameter. Although these values are slightly higher than typical Mound shards (Table 2), they are within the acceptable range.

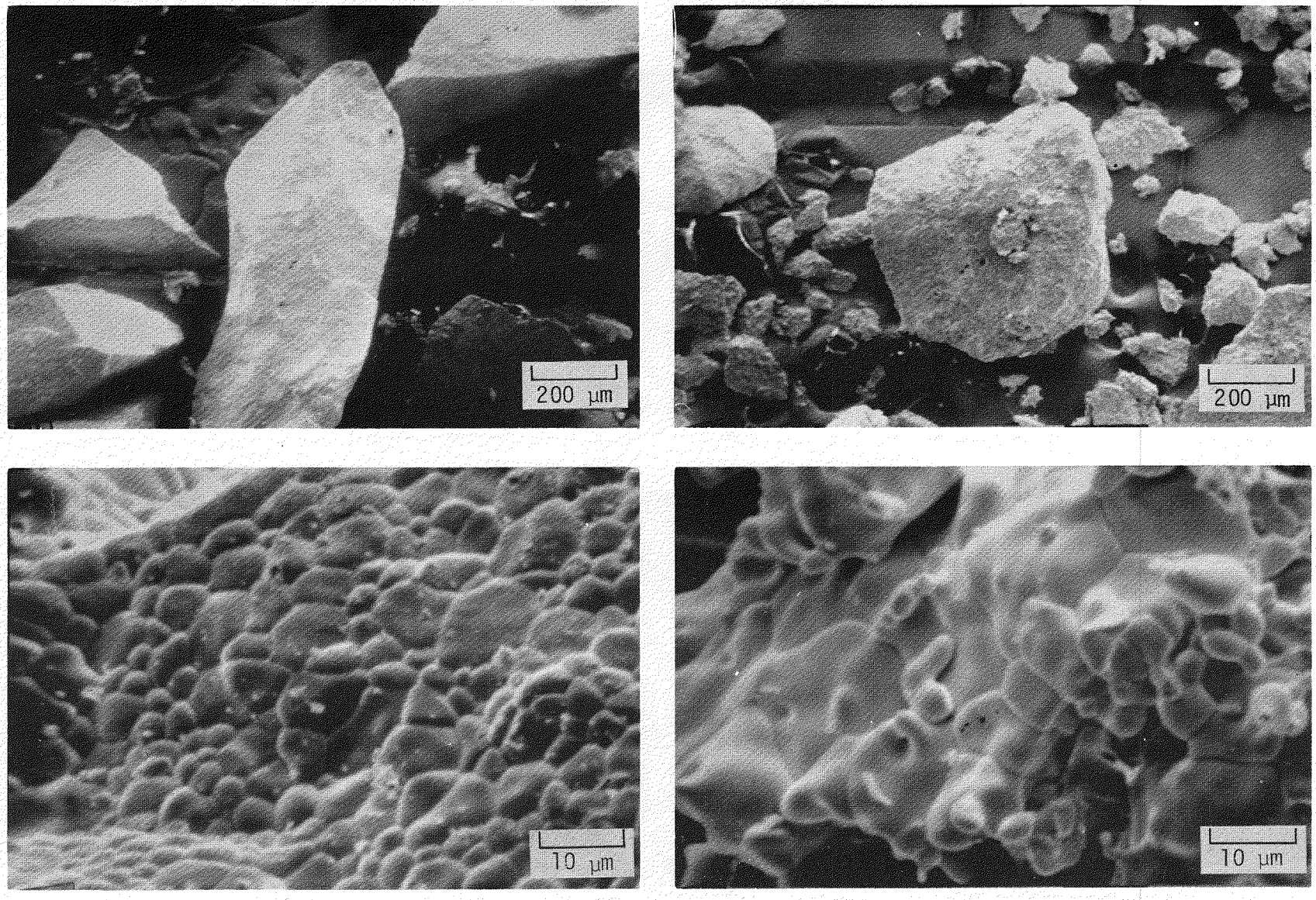

a. Shards Made in AMF

b. Shards Made in PuFF/PEF

FIGURE 20. Shards Made in Fabrication Tests in the AMF and PuFF/PEF

TABLE 4

Chemical Purity Analysis from Milliwatt Samples, ppm[a]

Element	*Specification*	*AMF Batch*	*PuFF/PE Batch*
Al	70	300[b]	55
B	10	10	6
Be	-	1	<1
Ca	250	180	150
Cd	25	<10	<10
Cr	150	6	75
Cu	50	4	10
Fe	500	380	230
Mg	50	39	35
Mn	50	6	10
Mo	-	5	5
Na	-	27	25
Ni	100	37	40
Pb	50	<5	<5
Si	100	190[b]	60
Sn	50	<10	<10
Zn	100	<4	<5

a. Values are average of spark source and emission spectroscopy.

b. Exceed specifications.

Production of Shards in PuFF/PEF

A 300-g batch of Milliwatt shards was fabricated in the PuFF and PEF facilities for proof-testing at MF. The objective was to produce shards representative of future Milliwatt fuel to be produced in the PuFF facility. PEF was utilized because the high-temperature sintering and washing steps could not be performed in PuFF. Production followed the flowsheet of Figure 19; batch sizes for process steps are compared in Table 3 with those of the AMF test.

Results of analyses of the shards made in PuFF/PEF are compared in Table 2 with the AMF shards. SEM examination of the shards revealed particles with a significantly different morphology (Figure 20b) and a greater fraction of small (<53 μm) particles than found in the AMF shards. As is apparent from Figure 20, the PuFF/PEF shards contained a greater number of small surface asperities, which contributed to the higher fines content of the fuel (Table 2). The PuFF/PEF shards had approximately the same average grain size, but appeared to be slightly less dense than the AMF shards. The packing density was slightly greater, which can be attributed to the greater fraction of small particles. Chemical impurity levels, measured by mass and emission spectroscopy, were all within specification (Table 4).

Cause of Deviant Morphology and Greater Fines Content

The cause of the undesirable change in surface morphology and increased fines content that occurred in transferring the process from the laboratory (AMF) to production facilities can be traced to scale-effects associated with cold pressing and sizing.

Production of shards in both the AMF and PuFF/PEF followed the same flowsheet, but deviated somewhat in batch sizes at various process steps (Table 3), especially the size of cold-pressed compacts. Evidently, this is where the problem occurred. The cold-pressed compacts made in PuFF were 75-g compacts compared 5-g compacts pressed in the AMF test. The 5-g compacts in the AMF were presintered and then broken into shards by a series of screening operations (2 mm, 1 mm, and 0.5 mm). On the other hand, to prevent any possible effect from self heating, the 75-g compacts in the PuFF were to be broken into less than ∿¼-in. fragments before presintering in PuFF and subsequent processing in PEF. However, upon receipt in PEF, the presintered pellet fragments were much smaller than expected. During sizing, 100% of the as-received material passed through the 2-mm screen, 40% passed through the 1-mm screen, and 20% passed through the 0.5-mm screen without any sizing or breakup. The presence of smaller particles was confirmed through SEM examination (Figure 21). Since particle size should not have changed appreciably during presintering or transfer from PuFF to PEF, apparently the shift to a smaller size distribution was established during initial breakup of the cold-pressed compact.

This premature establishment of particle morphology essentially eliminates the effectiveness of the presintering step and causes the increase in surface asperities. Ideally, the surface morphology of shards is controlled by the

presintering step. In an earlier flowsheet study (August 1975 report[9]), the presintering step was introduced to strengthen the cold press compact before sizing and, thus, control subsequent breakup and sizing into shards. Pellets, which were presintered, broke into shards with a size range and morphology similar to shards made in the AMF according to the flowsheet of Figure 19. Conversely, pellets which were not presintered broke into shards having numerous surface asperities, much like the shards produced in PuFF/PEF (Figure 22). In the case of the large 75-g compacts made in PuFF, surface morphology was established during breakup before presintering, thus obviating the desired effect of presintering. To prevent the premature and excessive breakup of cold-pressed pellets, several smaller compacts could be gang pressed and then presintered before breakup.

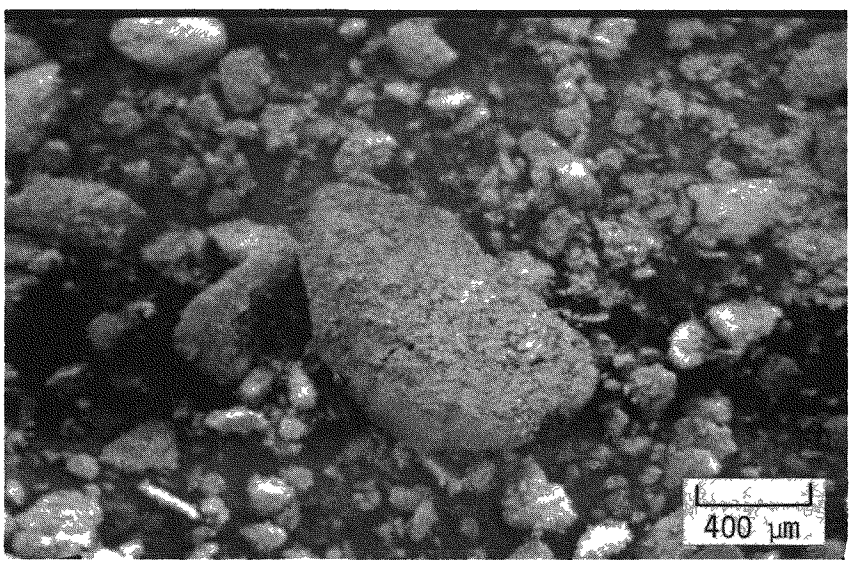

FIGURE 21. Presintered Material Before Sizing

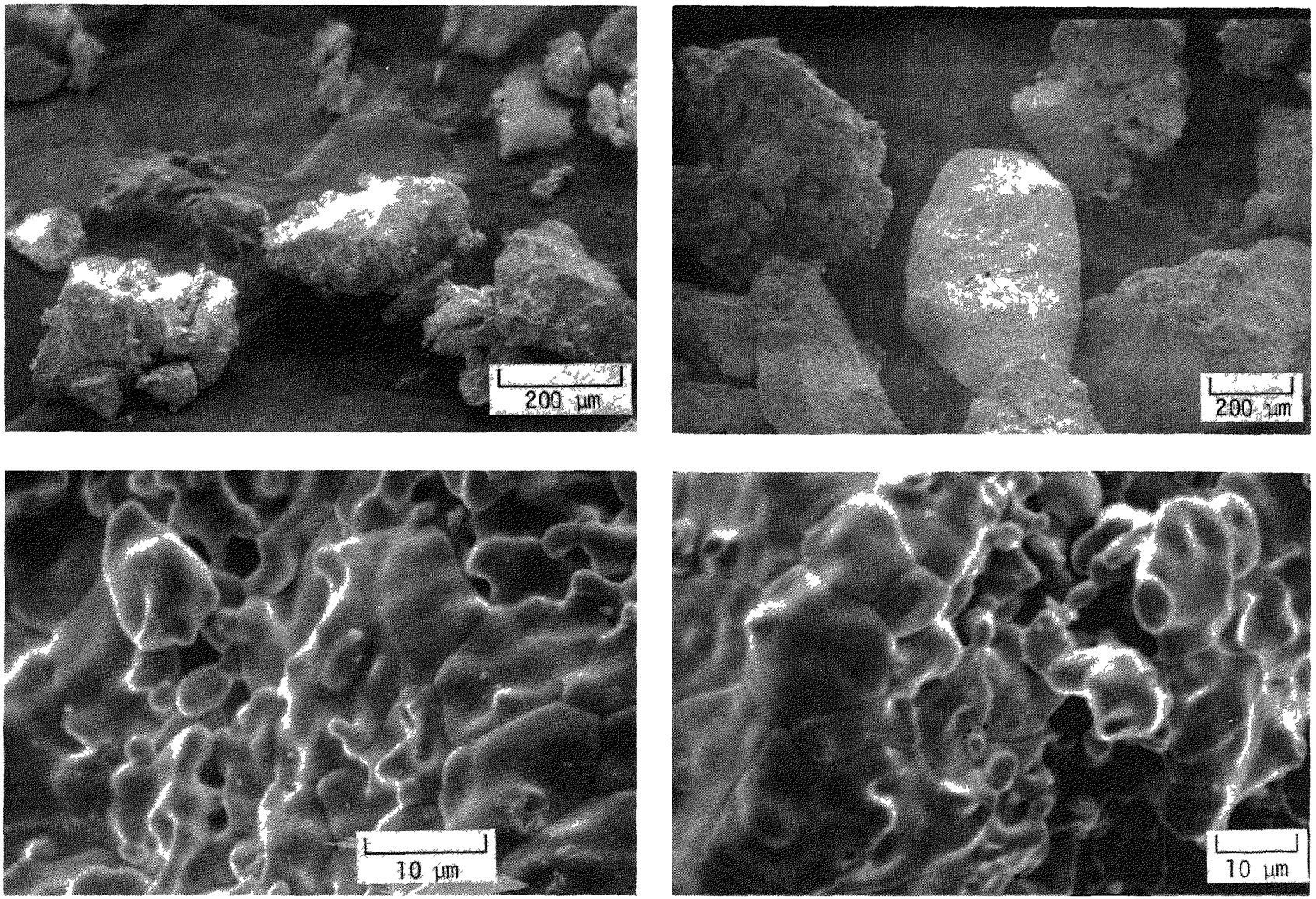

a. Shards Made in PuFF/PEF

b. Shards Made in Flowsheet Study (1975) Without Presintering Step

FIGURE 22. Comparison of Surface Morphology of Shards from PuFF/PEF and Shards from Flowsheet Study

REFERENCES

1. *Savannah River Laboratory Monthly Report,* ^{238}*Pu Fuel Form Processes, May/June 1978.* USDOE Report DPST-78-128-5/6, E. I. du Pont de Nemours & Company, Savannah River Laboratory, Aiken, SC (1978).

2. *Savannah River Laboratory Monthly Report,* ^{238}*Pu Fuel Form Processes, November/December 1977.* USDOE Report DPST-77-128-11/12, E. I. du Pont de Nemours & Company, Savannah River Laboratory, Aiken, SC (1978).

3. *Savannah River Laboratory Monthly Report,* ^{238}*Pu Fuel Form Processes, March/April 1978.* USDOE Report DPST-78-128-3/4, E. I. du Pont de Nemours & Company, Savannah River Laboratory, Aiken, SC (1978).

4. *Savannah River Laboratory Monthly Report,* ^{238}*Pu Fuel Form Processes, October 1976.* USERDA Report DPST-76-128-10, E. I. du Pont de Nemours & Company, Savannah River Laboratory, Aiken, SC (1976).

5. *Savannah River Laboratory Monthly Report,* ^{238}*Pu Fuel Form Processes, March 1977.* USERDA Report DPST-77-128-3, E. I. du Pont de Nemours & Company, Savannah River Laboratory, Aiken, SC (1977).

6. *Savannah River Laboratory Monthly Report,* ^{238}*Pu Fuel Form Processing, February 1976.* USERDA Report DPST-76-128-2, E. I. du Pont de Nemours & Company, Savannah River Laboratory, Aiken, SC (1976).

7. *Savannah River Laboratory Monthly Report,* ^{238}*Pu Fuel Form Processes, April 1976.* USERDA Report DPST-76-128-4, E. I. du Pont de Nemours & Company, Savannah River Laboratory, Aiken, SC (1976).

8. *Savannah River Laboratory Monthly Report,* ^{238}*Pu Fuel Form Processes, October 1977.* USDOE Report DPST-77-128-10, E. I. du Pont de Nemours & Company, Savannah River Laboratory, Aiken, SC (1977).

9. *Savannah River Laboratory Monthly Report,* ^{238}*Pu Fuel Form Processes, August 1975.* USERDA Report DPST-75-128-8, E. I. du Pont de Nemours & Company, Savannah River Laboratory, Aiken, SC (1975).

DISTRIBUTION

Copy No.

1 T. A. Dillon, Acting Director, Advanced Systems and Materials Production Division, U. S. Department of Energy

2 B. J. Rock, Acting Assistant Director, Office of Space and Terrestrial Systems, Advanced Systems and Materials Production Division, U. S. Department of Energy

3 J. J. Lombardo, Acting Chief, Power Systems Branch, Advanced Systems and Materials Production Division, U. S. Department of Energy

4 N. R. Thielke, Acting Chief, Technology Development Branch, Advanced Systems and Materials Production Division, U. S. Department of Energy

5 T. J. Dobry, Acting Chief, Safety and Isotope Fuels Branch, Advanced Systems and Materials Production Division, U. S. Department of Energy

6 R. F. Caudle, Asst. Secretary for Defense Programs, U. S. Department of Energy

7 V. C. Vespe, Albuquerque Operations Office

8 D. K. Nowlin, Albuquerque Operations Office

9 J. A. Chacon, Manager, Dayton Area Office

10 R. D. Baker, CMB, DO, Los Alamos Scientific Laboratory

11 S. E. Bronisz, CMB-5, MS-730, Los Alamos Scientific Laboratory

12 R. A. Kent, Los Alamos Scientific Laboratory

13 W. T. Cave, Monsanto Research Corporation

14 B. R. Kokenge, Monsanto Research Corporation

15 Technical Library, Sandia Laboratory, Albuquerque

16 M. K. Parson, Sandia Laboratory, Albuquerque

17 T. J. Young, Sandia Laboratory, Albuquerque

18 E. W. Williams, General Electric Company, Philadelphia

19 N. B. Elsner, Gulf General Atomic, San Diego

20 W. Pardue, Battelle Memorial Institute, Columbus, Ohio

21-26 Savannah River Operations Office, DOE

27-94 Savannah River Laboratory, TIS Files

96-97 Technical Information Center, Oak Ridge, TN

98 G. Linkous, Teledyne Energy Systems, Timonium, MD